INVESTIGATION OF STOCKBRIDGE DAMPERS FOR VIBRATION CONTROL OF OVERHEAD TRANSMISSION LINES

A THESIS SUBMITTED TO
THE GRADUATE SCHOOL OF NATURAL AND APPLIED SCIENCES
OF
MIDDLE EAST TECHNICAL UNIVERSITY

BY

HÜSEYİN KASAP

IN PARTIAL FULFILLMENT OF THE REQUIREMENTS
FOR
THE DEGREE OF MASTER OF SCIENCE
IN
MECHANICAL ENGINEERING

SEPTEMBER 2012

Approval of the thesis:

INVESTIGATION OF STOCKBRIDGE DAMPERS FOR VIBRATION CONTROL OF OVERHEAD TRANSMISSION LINES

submitted by **HÜSEYİN KASAP** in partial fulfillment of the requirements for the degree of **Master of Science in Mechanical Engineering Department, Middle East Technical University** by,

Prof. Dr. Canan Özgen _____
Dean, Graduate School of **Natural and Applied Sciences**

Prof. Dr. Süha Oral _____
Head of Department, **Mechanical Engineering**

Asst. Prof. Dr. Gökhan O. Özgen _____
Supervisor, **Mechanical Engineering Dept., METU**

Examining Committee Members:

Prof. Dr. S. Kemal İder _____
Mechanical Engineering Dept., METU

Asst. Prof. Dr. Gökhan O. Özgen _____
Mechanical Engineering Dept., METU

Asst. Prof. Dr. Ergin Tönük _____
Mechanical Engineering Dept., METU

Asst. Prof. Dr. Ender Ciğeroğlu _____
Mechanical Engineering Dept., METU

Sabri Çetin, M.Sc. _____
Lead Design Engineer, ASELSAN Inc.

Date: 14.09.2012

I hereby declare that all information in this document has been obtained and presented in accordance with academic rules and ethical conduct. I also declare that, as required by these rules and conduct, I have fully cited and referenced all material and results that are not original to this work.

Name, Last Name: Hüseyin KASAP

Signature :

ABSTRACT

INVESTIGATION OF STOCKBRIDGE DAMPERS FOR VIBRATION CONTROL OF OVERHEAD TRANSMISSION LINES

Kasap, Hüseyin
M.Sc., Department of Mechanical Engineering
Supervisor: Asst. Prof. Dr. Gökhan O. Özgen

September 2012, 92 pages

This thesis aims to examine the performance of Stockbridge dampers used to suppress aeolian vibrations on overhead transmission lines arising from the wind. In this respect, a computer program, based on the Energy Balance Method, is developed using MATLAB. The developed computer program has also a graphical user interface (GUI), which allows the program to interactively simulate Stockbridge damper performance for vibration control of overhead transmission lines. Field tests results obtained from literature are used in various case studies in order to validate and evaluate the developed software. Moreover, sample Stockbridge damper characterization tests, which then could be introduced to the software, are performed. A custom test fixture is designed due to its unavailability of commercial alternatives in the market. In the design of the test fixture, modal and transmissibility analyses are done by using ANSYS Workbench. To further validate the test setup, transmissibility test is done and consistent results with the transmissibility analyses are observed in the range of expected aeolian vibration frequencies. Finally, the stepped-sine and swept-sine tests are performed with and without damper for the characterization test, where the latter one is performed to

eliminate the negative effects of the test setup. Both tests yield almost same damper power dissipation curves.

Keywords: Stockbridge Damper, Aeolian Vibrations, Energy Balance Method, Damper Characterization Test, Tuned Vibration Absorbers

ÖZ

HAVAİ İLETİM HATLARI TİTREŞİM KONTROLÜ İÇİN STOCKBRIDGE TİTREŞİM SÖNÜMLEYİCİLERİ İNCELEMESİ

Kasap, Hüseyin
Yüksek Lisans, Makina Mühendisliği Bölümü
Tez Yöneticisi: Yrd. Doç. Dr. Gökhan O. Özgen

Eylül 2012, 92 sayfa

Bu tezde, havai iletim hatlarının rüzgardan kaynaklı aeolian titreşimlerini bastırmak için kullanılan Stockbridge titreşim sönümleyicilerinin performansını inceleme hedeflenmiştir. Bu kapsamda, MATLAB kullanılarak Enerji Denge Metoduna dayalı bir bilgisayar yazılım geliştirilmiştir. Geliştirilen bilgisayar yazılımı, GUI ile oluşturulan kullanıcı dostu bir arayüz ile desteklenerek Stockbridge titreşim sönümleyicilerinin havai iletim hatlarının titreşimlerini kontrol etmedeki performansını simule etme imkanı sağlanmıştır. Literatürde mevcut saha testleri kullanılarak çeşitli vaka çalışmaları ile geliştirilen yazılım doğrulanmış ve hesaplama performansı değerlendirilmiştir. Yazılıma girilebilecek örnek titreşim sönümleyici karakterizasyon testleri gerçekleştirilmiş ve bu kapsamda hazır alınamadığından dolayı bir test düzeneği tasarımı yapılmıştır. Test düzeneği tasarımı sırasında yapılan modal ve titreşim iletim analizleri, ANSYS Workbench ile gerçekleştirilmiştir. Tasarlanan test düzeneğini doğrulama çalışmaları kapsamında titreşim iletim test sonuçları, yapılan analizler ile tutarlılık sağlanmıştır. Son olarak, kademeli sinüs ve taramalı sinüs testleri gerçekleştirilmiş olup titreşim sönümleyici olmadan yapılan testler ile de düzeneğin test sonuçları üzerindeki olumsuz etkileri

ortadan kaldırılmıştır. Gerçekleştirilen her iki testte de titreşim sönümleyicinin güç dağıtma eğrileri birbirine çok yakın olarak elde edilmiştir.

Anahtar Kelimeler: Stockbridge Titreşim Sönümleyici, Aeolian Titreşimleri, Enerji Denge Metodu, Titreşim Sönümleyici Karakterizasyon Testi, Ayarlanabilir Titreşim Emiciler

ACKNOWLEDGMENST

The author wishes to express his sincere appreciation to his supervisor Asst. Prof. Dr. Gökhan O. ÖZGEN for the support and encouragement during his research activities.

The author would like to thank to ASELSAN, Inc. and his manager Mr. İhsan ÖZSOY, for his support and let to use experimental facilities of mechanical/optical design department. Many thanks go to his colleague Güvenç CANBALOĞLU for the endless support and patience during the laboratory tests. The author would like to express his appreciation to his colleagues Sabri ÇETİN and Mustafa ÖZTÜRK for their valuable support and understanding.

The author would like to thank to Asst. Prof. Dr. Ender CİĞEROĞLU for supplying the Stockbridge damper that is used during the damper characterization tests.

Lastly the author would like to express his endless gratitude to his family for their love, support and faith in him. Finally and may be most importantly, the author is indebted to Dilem YILDIRIM for always being there to share his laughs, successes and worries.

TABLE OF CONTENTS

LIST OF TABLES

TABLES

LIST OF FIGURES

FIGURES

LIST OF SYMBOLS

Latin Symbols

A	: Vertical displacement amplitude (single amplitude)
(A/D)	: Relative vibration amplitude
c	: Damping coefficient
c_w	: Wave velocity
C_L	: Lift coefficient
D	: Conductor diameter
E_o	: Young's modulus for the outer-layer strand material
E_{wind}	: Wind energy
EI	: Flexural rigidity of the conductor
f	: Lock-in frequency
f_n	: Natural frequency of the cylinder
f_{vs}	: Vortex-shedding frequency
$fnc(A/D)$	: Reduced power function
F_a	: Aerodynamic lift force
$F_{damp.}$	: Damper force obtained from the characterization test
F_L	: Magnitude of lift force
F_{TVA}	: TVA reaction force
k	: Stiffness
k_w	: Wave number
K	: Proportionality factor
l_1	: Distance between the damper and the suspension clamp
l, m and n	: Conductor self-damping exponents

L	: Span length
m	: Mass
m_L	: Conductor mass per unit length
p	: Bending stiffness parameter
$P_{char.}$	: Damper power obtained from the characterization test
$P_{cond.}$	: Power dissipated by the conductor
$P_{damp.}$	: Power dissipated by the vibration damper
P_{wind}	: Power brought into the system by the wind
r	: Mode number
Re	: Reynolds number
St	: Strouhal number
V	: Velocity of the wind
V_{clamp}	: Clamp velocity of the Stockbridge damper
V_r	: Reduced velocity
w	: Vibration frequency
w_p	: Vibration frequency of the primary structure
w_t	: Vibration frequency of TVA
x_t, y_t	: TVA position coordinates
Y_b	: Peak-to-peak displacement amplitude of the conductor
z	: The transverse displacement of the cylinder
Z	: Damper impedance

Greek Symbols

α	: Phase angle between force and velocity at the shaker test
d_o	: Diameter of outer-layer strand

ε_b	: Bending strain of the conductor
λ	: Wave length
θ	: Phase angle between force and displacement of the cylinder
ρ	: Density of the fluid
μ	: Dynamic viscosity of the fluid

Abbreviations

EBM	: Energy Balance Method
FBM	: Force Based Method
FRF	: Frequency Response Function
GUI	: Graphical User Interface
ISWR	: Inverse Standing Wave Ratio Test Method
PT	: Power Test Method
TVA	: Tuned Vibration Absorber

CHAPTER 1

INTRODUCTION

Aeolian vibrations, which are wind-induced vibrations due to the shedding of vortices, cause damages that negatively affect the service life of the overhead transmission lines. In order to deal with these negative effects of aeolian vibrations, Stockbridge dampers are the most conveniently and commonly used dampers. In this context, this thesis aims to investigate the performance of Stockbridge dampers which are designed to minimize the negative effects of aeolian vibrations and extend the life of overhead transmission lines. In order to reach thesis objectives, a computer program based on a validated analytical model is built up by using MATLAB. Sample characterization tests, by which the damping ability of the Stockbridge damper could be introduced to the software, are performed with a design of a test fixture. In the design and validation steps of the test fixture, transmissibility analysis is done by using ANSYS Workbench and the corresponding test is performed in the laboratory. Finally, the stepped-sine and swept-sine tests are performed with and without damper for the characterization test of the Stockbridge damper.

1.1 Summary of the Literature Review

In suspended conductors, wind can generate three major modes of vibration which are gallop, aeolian and wake-induced oscillations. Among them, aeolian vibration, which is the most destructive one, causes damages in the form of abrasion or fatigue failures over a period of time. This vibration activity becomes more severe in the coldest month of the year when the tensions reach the highest values [1], [2].

In order to overcome these crucial damages of aeolian vibrations, many dampers are designed. Among them the most commonly used ones are Stockbridge dampers, torsional dampers, Elgra dampers, spring-piston dampers and spiral dampers [3], [4]. The Stockbridge dampers have many advantages over the mentioned types of dampers. One of these advantages is that it can dissipate vibrations in any direction. Secondly, the Stockbridge damper can be used on the conductors in a wider diameter range compared to other damper alternatives and finally, they can be tuned to be effective over a wider range of frequency.

As stated in the international standard IEC 61897, the effectiveness of Stockbridge dampers can be evaluated by the field tests, the laboratory tests and the analytical models [5]. In the field tests, most vibration recorder devices have electronic circuitry and their accuracy can be affected by temperature changes, electrical noise from the environment, component aging and calibration errors. Also, there are negative effects of the recorder mass and the rotational inertia. Field tests should be long enough to cover several weather conditions (minimum 3 months) which should be close to each other with and without the Stockbridge dampers [6], [7]. In the laboratory tests, on the other hand, free span length should be minimum 30 m [5], [8], [9]. Moreover, same problems due to the electrical noise from the environment, component aging and calibration errors also exist in laboratory tests. On the other hand, analytical methods always estimate the maximum vibration amplitudes of the conductor while actual vibration levels observed in the field may not reach the analytically calculated maximum values. Besides, analytical methods, which are based on the wind tunnel tests to estimate the input wind power and the dissipated power by the conductor due to the self-damping, are altered with the test conditions. However, analytical methods are fast and easy to apply though they should be validated against the laboratory results or the field test results [5].

1.2 Motivation and Objectives

Most of the foreign suppliers of Stockbridge dampers develop their own software which is based on an analytical model but they do not share them with their purchasers. Suppliers give only general instructions on their catalogues about the usage of the Stockbridge dampers and this is provided with a table representing only the clamp range to choose a product suitable to the diameter of the target conductor. According to the environmental conditions and the properties of the conductors, suppliers give support to their customers about the number and position of the dampers needed to protect the conductors. By this way, purchasers are not able to compare the performances of different products while choosing the proper Stockbridge damper for their specific condition.

On the other hand, most of the domestic suppliers of Stockbridge dampers in Turkey do not have a comprehensive theoretical background to develop their own software to check the acceptance criteria about the effectiveness evaluation stated in the international standards for their own Stockbridge damper designs. In addition, most of them do not have enough facilities for either laboratory tests or field tests to check this acceptance criterion. Therefore, they are generally inspired by the existing Stockbridge models in the market to extend the variety of their products.

In this thesis, it is aimed to evaluate the effectiveness of the Stockbridge dampers by a computer program with a friendly graphical user interface (GUI) which is built up by using MATLAB. For this purpose, an appropriate analytical model is chosen for the performance evaluation of the Stockbridge dampers placed on the overhead transmission lines. Afterwards, existing field test results are used to validate the developed software.

Sample Stockbridge damper characterization tests are also performed which could then be introduced to the software to represent the capacity ability of the Stockbridge damper. For this purpose, a test fixture is required and due to its unavailability in the

market, it is designed and produced as a part of this thesis work. Modal and transmissibility analyses are performed on the proposed fixture design by using ANSYS Workbench in the conceptual design steps in order to constitute a basis for the detailed design of the test fixture and they are repeated to ensure sufficient dynamic performance of the text fixture before the production. Before the Stockbridge damper characterization tests, the produced test fixture is validated by performing a transmissibility test of the fixture alone in laboratory environment.

The outcome of this thesis study may enable purchasers to compare the performances of different suppliers' dampers to make the most convenient choice. More specifically, by this study, performance of the Stockbridge dampers can be compared for any condition such as conductor type, diameter, mass per length, tension, span length and average wind velocity. Number and position of the damper on the overhead transmission lines can also be altered by using the user friendly MATLAB interface to reach the optimum performance for mentioned conditions or to prepare the tables for the practical usage of the Stockbridge dampers.

Finally, outcome of this study can be used for the acceptance criterion of the Stockbridge dampers by the purchasers. It will also enable suppliers to provide performance guarantee of their products to the purchasers before the sale.

1.3 Outline

The outline of the thesis is as follows. In chapter 2, existing literature related to the wind induced-vibrations, vibration damping devices, tuned vibration absorbers and overhead transmission line field vibration measurements are provided. Due to the focus on the Stockbridge dampers and aeolian vibrations, relevant literature is investigated in more detail.

Chapter 3 discusses and compares two analytical methods, which are Forced Based Method and Energy Balance Method. Due to the focus being mainly on the Energy Balance Method, it is discussed in more detail, with the underlying assumptions, limitations and existing approaches for the power brought into the system by the wind, dissipated power by the self-damping of the conductor and the dissipated power by Stockbridge damper. Bending strain and stress of the conductor at the suspension clamp and the conductor displacement are also discussed at the end of the chapter.

Chapter 4 provides a discussion for the conceptual and the detailed design of the software together with the inputs and the outputs. The interface of the software is presented in more detail with the capabilities of the software. Employing existing field tests, the validation step of the software is completed with and without damper cases. Besides the field tests, a number of case studies are utilized to measure the accuracy of the software.

In chapter 5, the conceptual and the detailed design of the test setup are given together with the modal and the transmissibility analyses. The performed transmissibility test is examined further in the validation step of the test setup and the results are discussed at the end of the chapter.

Chapter 6 explains the procedure of the damper characteristic test, which is stated in the international standard IEC 61897. After a brief introduction of the test equipments, performed stepped-sine and swept-sine tests are explained for with and without damper cases and the comparison of the test results are presented at the end of the chapter. Finally, chapter 7 concludes the thesis.

CHAPTER 2

LITERATURE REVIEW

In this chapter, existing literature related to the wind induced-vibrations, vibration damping devices, tuned vibration absorbers and field vibration measurements are discussed. Due to the focus on the Stockbridge dampers and aeolian vibrations, related literature is investigated in more detail.

2.1 Wind-Induced Vibrations

Overhead transmission lines are continuously subjected to wind forces that shorten the service life by cyclic conductor motions. These wind forces generate three major modes of oscillation in the suspended conductors as seen in Figure 2.1 [1]:

- *Gallop* has an amplitude measured in meters and a frequency range of 0.08 to 3 *Hz*.
- *Wake-induced (subspan) oscillation* has an amplitude of centimeters and a frequency range of 0.15 to 10 *Hz*.
- *Aeolian vibration* (flutter) has an amplitude of millimeters to centimeters and a frequency range of 3 to 150 *Hz*.

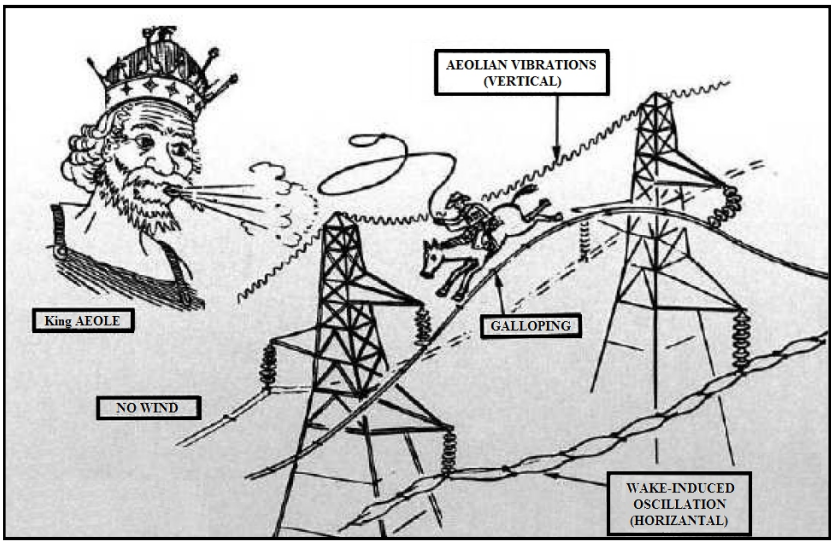

Figure 2.1 Wind-induced vibrations [10]

Galloping commonly occurs when there is an asymmetrically ice-coated conductor in the wind flow with a speed above 15 *mph* (7 *m/s*). The ice coating creates irregular edges and surfaces which disturbs the wind flow over the conductor. Peak-to-peak amplitudes can be higher than the sag of the mid-span and this causes a flashover between the phases (sometimes between the phase and the ground) which damages the conductors. In addition, galloping can also damage the towers with their severe amplitudes as seen in Figure 2.2 [2], [10], [11].

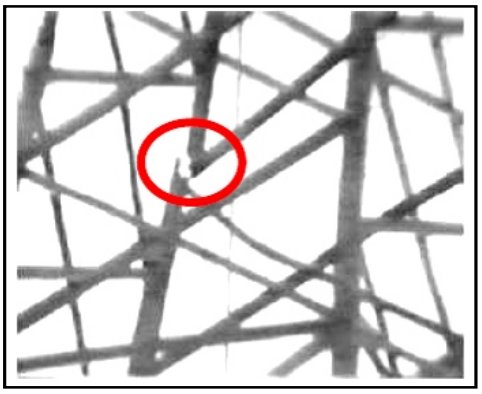

Figure 2.2 Galloping damage on a tower [10]

Wake-induced oscillation, which is associated with bundled conductors, is caused by forces that originated by the shielding effect of the wind side conductors in the wind flow of 15 to 40 *mph* (7 to 18 *m/s*) [2], [11].

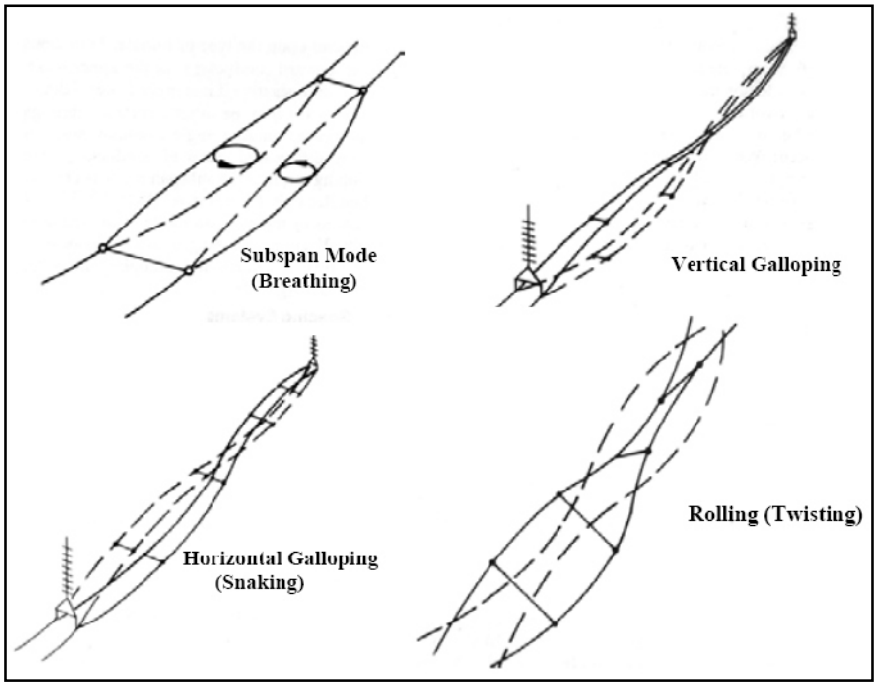

Figure 2.3 Modes of the wake-induced oscillations [2]

There are breathing, vertical galloping, snaking and rolling modes of the wake-induced oscillations as illustrated in Figure 2.3. Vertical galloping, snaking and rolling modes are the entire span motions, on the other hand, breathing is a sub-span behavior of the conductor. These vibration modes create forces and torques on the conductor and their accessories but they are limited to wear rapidly [2], [10]. Since the focus of this thesis is on the control of aeolian vibrations, they are discussed in more detail in the next subsection.

2.2 Aeolian Vibrations

It is believed that term aeolian originates from Greek mythology and in modern times it is used to represent a particular type of wind-induced vibrations, aeolian vibrations [12].

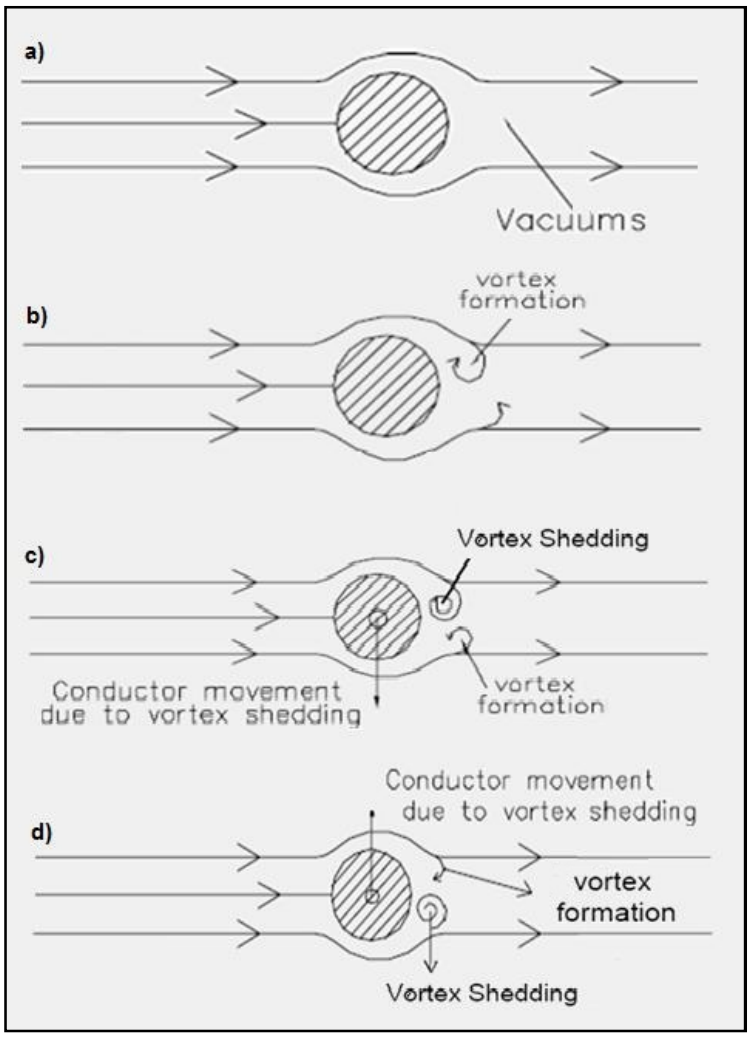

Figure 2.4 a) vacuum creation, b) the first vortex formation, c) movement of the conductor d) movement of the conductor in the reverse direction [13]

Aeolian vibrations occur when a smooth wind flow of 2 to 15 *mph* (1 to 7 *m/s*) interacts a conductor. When this happens, air accelerates to go around the conductor

and then separates behind it as seen in Figure 2.4. This motion creates a low-pressure region at the opposite side of the conductor and the air shows a tendency to move into this vacuum zone. This is the vortex shedding action that creates an alternating pressure imbalance causing the conductor to move up and down at ninety degree angle to the flow direction. On the other hand, winds higher than 15 *mph* usually contain a considerable amount of turbulence and decrease the generation of the vortices [13], [14], [15].

The main factors effecting the aeolian vibrations are the span length, the tension and the mechanical impedance of the conductor. The amount of mechanical energy passing through the condcutor increases with the span length. An increase in tension, on the other hand, raises the vibration tendency of a conductor due to a decline in its natural self-damping. Finally, the mechanical impedance is determined by the mechanical and material properties of the conductor. Therefore, maximum vibration amplitude is generally equal to the conductor diameter when the most serious aeolian vibrations occur by steady winds at the long spans with high conductor tensions in the smooth terrain [10], [12].

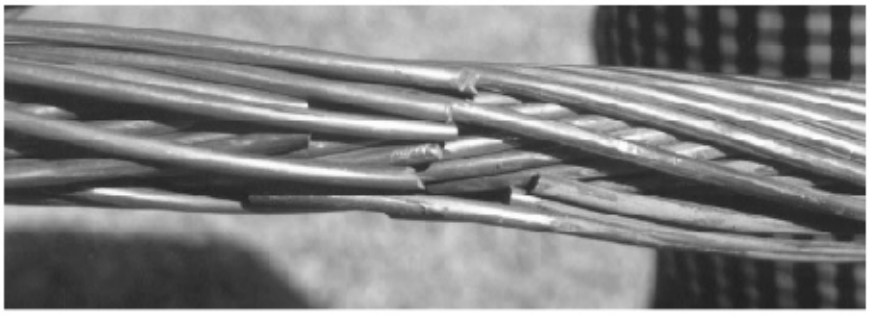

Figure 2.5 Fatigue failure of conductor strands at the suspension clamp [16]

Aeolian vibrations create dynamic bending stresses on the conductor which cause the fatigue failure of strands at the supporting locations when the endurance limit of the

strands is exceeded. As seen in Figure 2.5, strands in the outer layer fail firstly since they are subjected to the highest level of bending stresses [10], [15].

Failure time depends on the magnitude of the bending stresses and the number of bending cycles that exceed the endurance limit of the strands. During warmer months, bending stresses are generally below the endurance limit but they usually exceed the endurance limit during the winter since the tensions are higher that reduce the motility of the conductor (self-damping) [2].

2.3 Vibration Damping Devices

In order to deal with the negative effects of aeolian vibrations, a variety of impact and tuned dampers are designed. Among them the most commonly used ones are torsional dampers, Elgra dampers, spiral dampers, spring-piston dampers, pneumatic dampers and Stockbridge dampers [3], [4].

Torsional dampers, Elgra dampers and spiral dampers (Figure 2.6) are classified as the impact dampers that use collision energy to dissipate the vibration energy. Torsional dampers simply increase the interstrand friction of the conductor as a result of the torsional motion produced by the offset weights when the conductor vibrates. They are effective on conductors smaller than about 12.5 *mm* in diameter $(1/2")$.

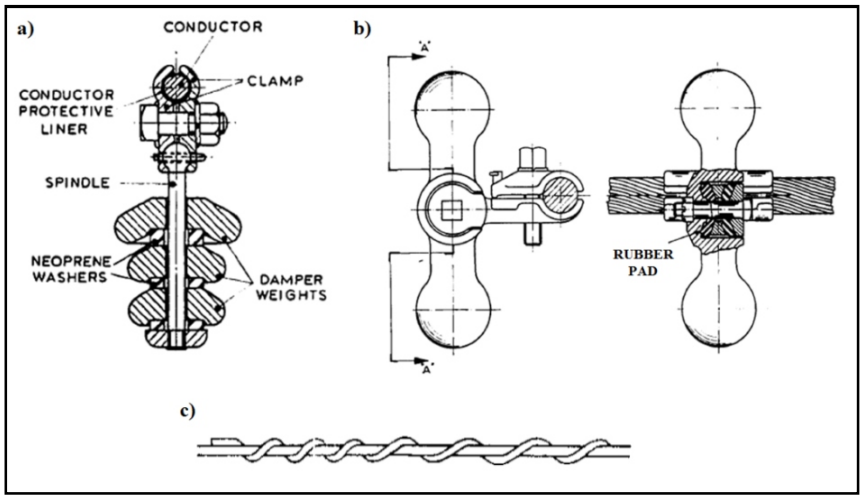

Figure 2.6 Impact dampers a) Elgra damper, b) torsional damper and c) spiral vibration damper [3], [4]

Unfortunately, torsional dampers are efficient in a narrow frequency range and have a tendency to freeze up in the winter. Elgra dampers, on the other hand, are effective to give different frequency responses with their variety of plate-type weights. In a vibration activity, these weights move up and down on the spindle to dissipate the energy by the help of Neoprene washers but they are very noisy and cause excessive wear at the connection point of the conductor [3], [4].

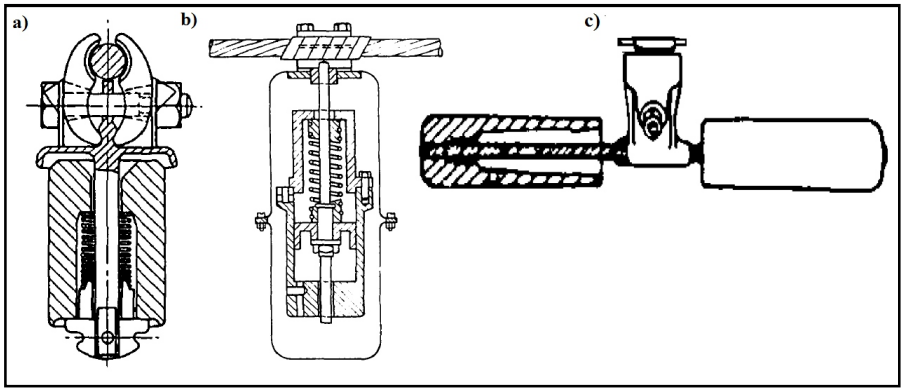

Figure 2.7 Tuned dampers a) spring-piston damper, b) pneumatic damper and Stockbridge damper [3], [4]

Spiral dampers are geometrically separated from the torsional dampers and the Elgra dampers but they also suppress the vibration by impacting against the conductor. Generally, spiral dampers are effective in the frequency range of 100 *Hz* to 300 *Hz* and these frequencies occur on conductors smaller than about 16 *mm* in diameter $(5/8'')$. Since the spiral damper suppresses the vibrations within its length, it should be made long enough to cover as many vibration loops as it can [4].

Spring-piston dampers, pneumatic dampers and Stockbridge dampers (Figure 2.7) are classified as the tuned dampers which are effective when their natural frequency coincide with the excitation frequency of the conductor and this working principle is discussed in more detail in the next subsection. Unlike the spring-piston dampers and the pneumatic dampers, the Stockbridge dampers can be tuned to be effective over a wide range of frequency and they can dissipate vibrations in any directions [3]. Since the Stockbridge dampers are the focus of this study, they are discussed in more detail in subsection 2.5.

2.4 Tuned Vibration Absorbers

During a mechanical design, the damping of structural components and materials is often a considerably missed criterion that causes many mechanical failures in the long term. In this sense, the use of tuned vibration absorbers (TVA) is one of the solutions to the vibration problems.

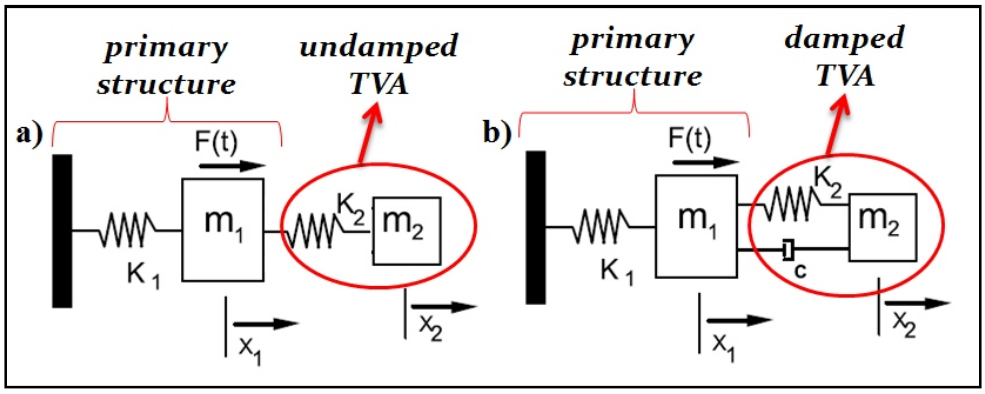

Figure 2.8 Primary structure with a) undamped, b) damped TVA adopted from [17]

TVA is a device that suppresses the vibration of a primary structure by transferring the energy to a secondary mass and can be in the case of damped or undamped as illustrated in Figure 2.8. If the vibration response is dominated by a single frequency that is the same frequency as a nearby disturbance source, using an undamped TVA is probably sufficient which consists only a mass and a spring. On the other hand, if the vibration is dominated by a single frequency and that frequency corresponds to a resonance, then using a damped TVA is more appropriate which consists of a mass, a spring and a damping device. In these vibration absorbers, mass is the inertia element, spring is the resilient element and the damping is the energy dissipating element [18].

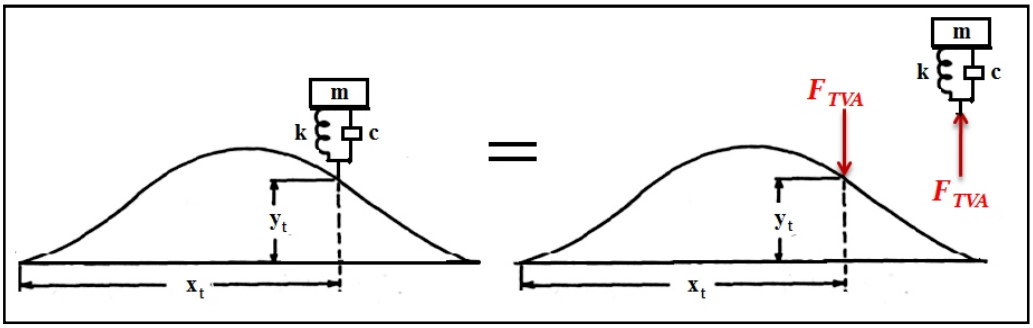

Figure 2.9 TVA reaction force on the surface of primary structure adopted from [19]

When a TVA is attached to the vibrating surface of a structure, the motion of the TVA is much greater than the primary structure. At the point of attachment, the reaction force is transmitted back on the structure and TVA resists the motion of the structure at this point as seen in Figure 2.9.

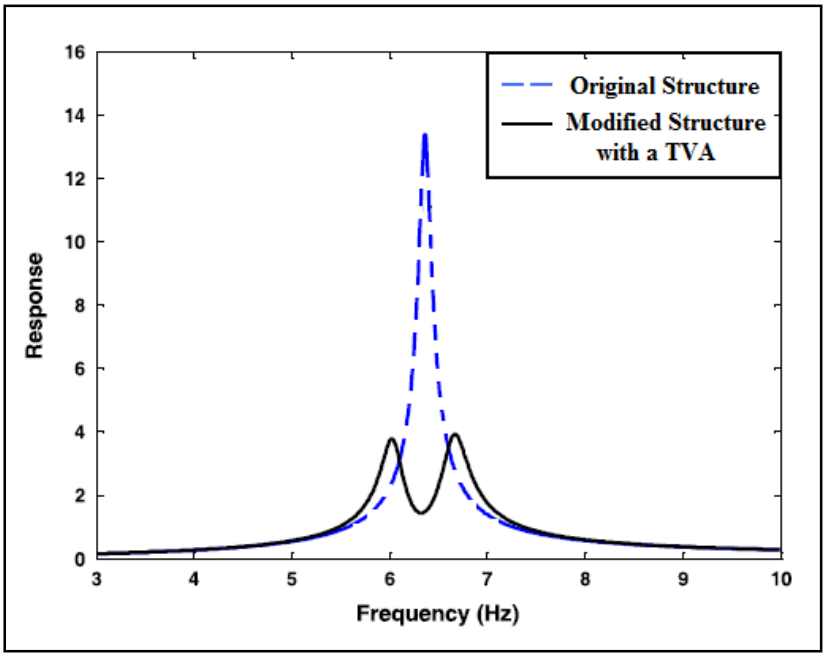

Figure 2.10 Frequency Response Function (FRF) of the original and modified structure by adding a TVA with an intermediate value of damping adopted from [20]

The effectiveness of a TVA is dependent on the damping ratio, the mass ratio and the frequency ratio of the TVA to the primary structure [21]. As illustrated in Figure 2.10, once a properly tuned vibration absorber with an intermediate value of damping is added to a primary structure, it splits the natural frequency of the primary structure and the modified structure has two new resonances that are lower than the original one. In the case of adding an undamped TVA, where the damping of the TVA is zero, resonance occurs at the two undamped resonant frequencies of the modified structure. However, when the damping of the TVA is infinite, the modified structure

becomes one degree of freedom system with the stiffness of original one (k_1) and the mass of combined system (m_1+m_2) due to the effect of locking the TVA's spring (k_2). Once the mass of the TVA increases, the separation between the two new frequencies of the modified structure becomes wider which generally means that the TVA becomes effective over a broader range of frequencies [20].

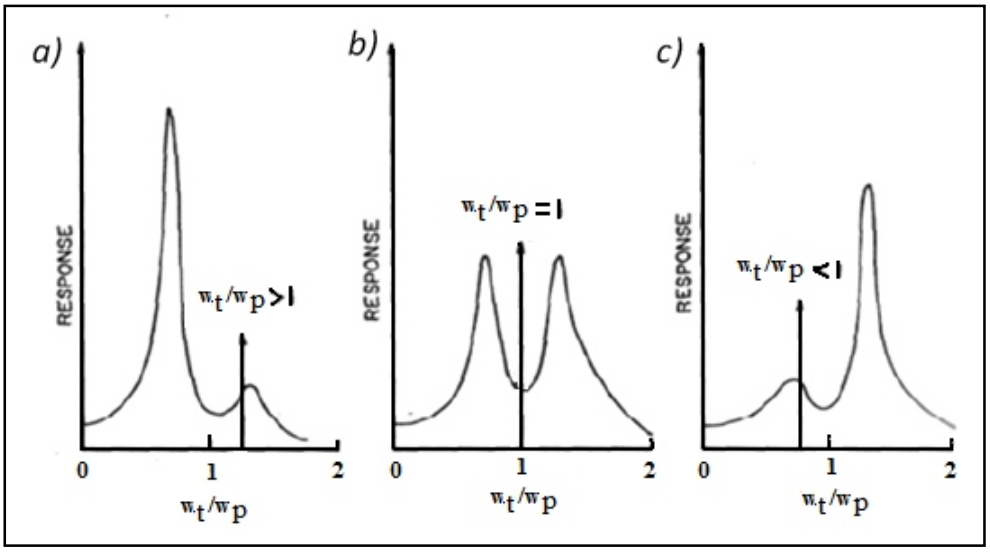

Figure 2.11 FRF of a) overtuned, b) tuned, c) undertuned systems adopted from [19]

The response of the primary structure can be suppressed effectively when TVA's natural frequency is tuned to the natural frequency of the primary structure. In Figure 2.11, the cases of overtuned, tuned and undertuned systems are given where w_t / w_p is the ratio of natural frequency of the TVA to the natural frequency of the primary structure.

2.5 Stockbridge Damper

Stockbridge dampers are used to suppress aeolian vibrations on overhead transmission lines caused by the wind. It works as a damped TVA with multiple

resonant frequencies and consists of two masses at the ends of a short length of cable (messenger) clamped to the main cable as seen in Figure 2.12.

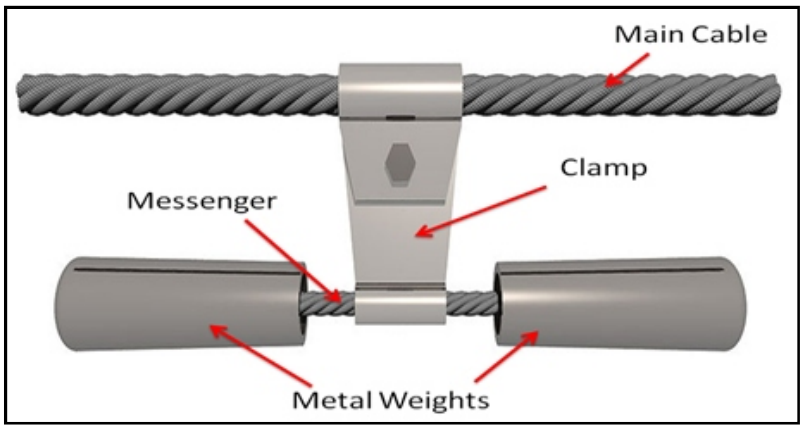

Figure 2.12 Modern design Stockbridge damper with metal weights [1]

George H. Stockbridge invented the Stockbridge damper in the 1920s while working as an engineer for Southern California Edison. US patent 1675391 was also obtained on 3 July 1928 for a "vibration damper" by him. In this design, concrete blocks were placed symmetrically on the messenger as seen in Figure 2.13 [22].

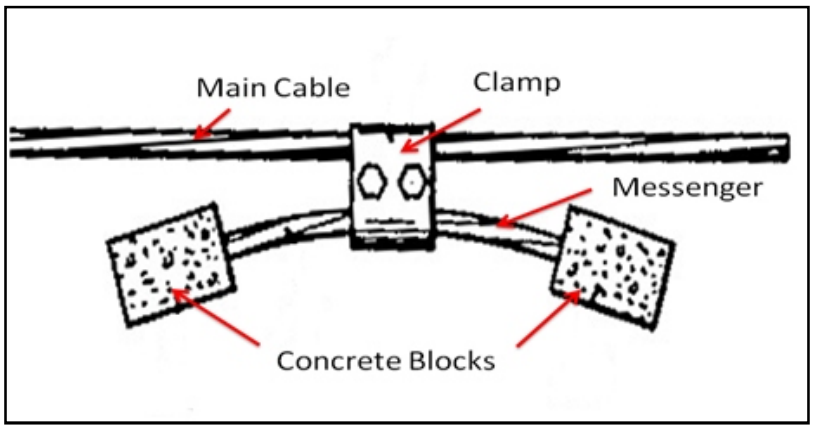

Figure 2.13 Original concrete block design of Stockbridge damper [22]

2.5.1 Working Principle of Stockbridge Damper

When the damper is placed on a vibrating conductor, vibrations pass down through the clamp and reach to the weights. Movement of the weights will produce bending of the messenger, which causes the individual wire strands (Figure 2.14) to rub together (interstrand friction) and dissipate energy. This action constitutes the damping effect of the Stockbridge damper. In the early designs, the messenger consists of 7 individual wire strands but once the importance of the messenger is realized, it has been started to construct modern designs with 19 individual wire strands on their messenger [3], [23].

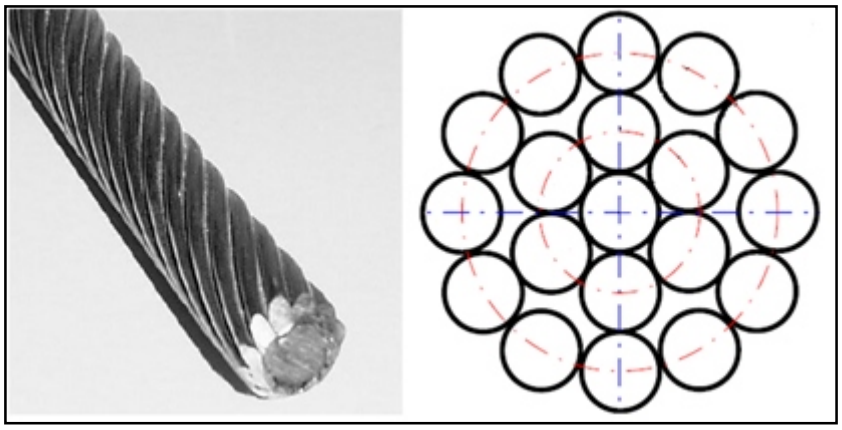

Figure 2.14 The messenger (left) and the individual wire strands (right) [24]

Appropriate choice of mass blocks, messenger length and stiffness of the damper increases the mechanical impedance of the cable which in turn decreases oscillations of the main cable substantially. In a symmetrical Stockbridge damper, each of weight has two identical degrees of freedom, which correspond to first and second modes of the damper, in the vertical plane. As illustrated in Figure 2.15, the outer ends of the damper weights have the maximum displacement in the 1st mode and the inner ends of the damper weights have the maximum displacement in the 2nd mode [12].

On the other hand, asymmetric placement of the weights on the messenger and the usage of two different weights on the Stockbridge damper provide the broadest effective frequency range in more advance designs.

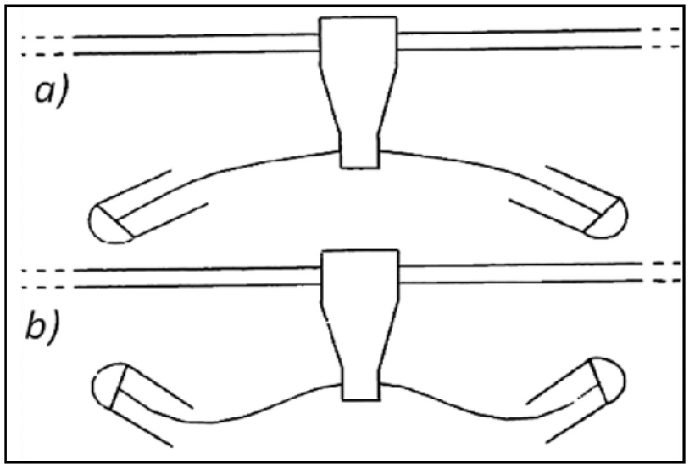

Figure 2.15 Representations for a) the first mode, b) the second mode of a symmetrical Stockbridge damper [12]

The ends of a power line span, where it is clamped to the transmission towers, are at most risk. Generally, there are two dampers per span which are at anti-nodes where the amplitude of the standing wave is a maximum. More than two dampers can be also installed if necessary on longer spans.

2.5.2 Acceptance Criteria

The effectiveness evaluation of Stockbridge dampers can be performed as stated in the international standard IEC 61897 by means of one of the following methods:

- laboratory test
- field test

- analytical method

The acceptance criterion of the laboratory test is that the power transferred from the shaker shall exceed the assumed wind power input for each test frequency during the test [5]. Laboratory tests of Stockbridge dampers are performed according to the IEE Std. 664-1980 which describes the procedure for determining the performance of vibration damping systems [8]. With this standard, conductor self-damping measurements have to be performed as described in IEE Std. 563-1978 and this standard uses two methods [9]:

- Power Test (PT) method in which the conductor is enforce to the resonant vibrations by a shaker and the total power dissipated by the conductor is measured at the input point.
- Inverse Standing Wave Ratio Test (ISWR) method which is based on the measurement of the power flow through the conductor in the resonant conditions.

The acceptance criterion of the field test is that the measured bending amplitudes or strains are considered and they shall be agreed between the purchaser and the supplier by the reference of the IEE Std. 1368-2006 or to equivalent publications [5]. According to this standard, a set of widely used criteria is the following [6]:

- No more than 5% of bending amplitude cycles can pass the endurance limit.
- No more than 1% of the cycles can pass 1.5 times of the endurance limit.
- No cycles can pass two times of the endurance limit.

The details of the field test are explained in the subsection 2.6. Finally, the focus of this study, analytical method, is discussed in more detail in Chapter 3

2.6 Field Vibration Measurements

Since the field tests take long time and have expenditure, there should be serious concerns about the conductors to be tested. Field vibration measurements are performed according to the IEE Std. 1368-2006 for the overhead transmission lines with the following aims [6]:

- To explore the reason behind of visible conductor fatigue damage.
- To monitor the existing vibration levels.
- To specify the possible future fatigue damage of the conductor.
- To investigate the damping performance of conductors and any attached vibration damping system.

Measurements are collected with the typical vibration recorders illustrated in Figure 2.16. Generally, the vibration recorders sample the conductor vibration for a few seconds in every 15 minutes [25].

Figure 2.16 Typical vibration recorders [26]

Bending amplitude is the peak-to-peak amplitude of the conductor displacement relative to the supporting clamp and it is measured at 89 *mm* (3.5") from the last point of the contact between the conductor and the clamp as seen in Figure 2.17.

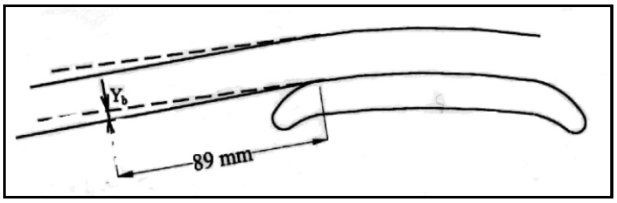

Figure 2.17 Bending amplitude, Y_b [6]

In order to see only the alternating stress (bending stress) effects, which cause the fatigue failure, without the inertial forces caused by the conductor's acceleration during the vibration activity, the data should be taken close enough to the clamp. On the other hand, it is necessary to be far enough from the clamp to measure the bending amplitudes accurately. So, it is found that the optimum place is the 89th *mm* by the experimental studies as illustrated in Figure 2.18 [6], [27].

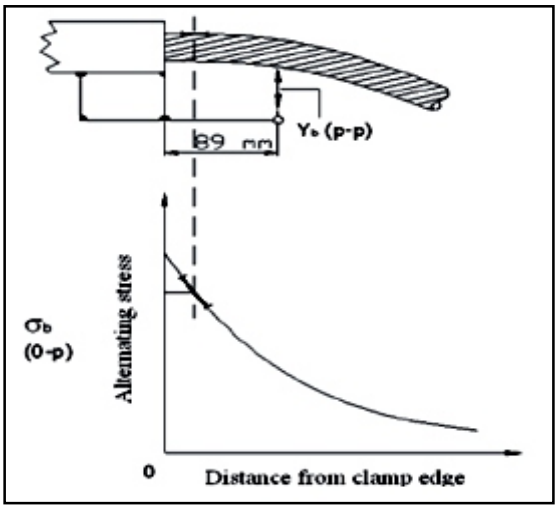

Figure 2.18 Graph of alternating stress vs. distance from the clamp edge [6]

CHAPTER 3

DEVELOPMENT OF THE ANALYTICAL MODEL

In this chapter, two analytical methods, which are Force Based Method and Energy Balance Method, are discussed and compared. Due to the focus on the Energy Balance Method, it is discussed in more detail, namely the underlying assumptions, limitations and existing approaches for the power brought into the system by the wind, dissipated power by the self-damping of the conductor and the dissipated power by Stockbridge damper are examined, respectively. Bending strain and stress of the conductor at the suspension clamp and the conductor displacement are also discussed at the end of the chapter.

3.1 Analytical Methods

There are two methods available to deal with the vibration amplitudes of the cables caused by the aeolian vibrations and these are Force Based Method (FBM) and Energy Balance Method (EBM). Force Based Method is based on the balance of the vortex-induced lift force, conductor self-damping force and the force of the damper. On the other hand, Energy Balance Method is based on the power balance among the power of the wind, the power dissipated by the conductor due to conductor's self-damping and the power dissipated by the vibration damper [12].

Both of them can use the maximum displacement amplitude and the bending amplitude of the conductor to compare the conditions with and without damper. Unlike Energy Balance Method, Force Based Method accounts for the travelling

wave effects, the contributions from other modes of vibration, flexural rigidity of the conductor and the damper mass [12].

When the results of two methods are compared, they are nearly the same at the damper positions close to the end of the span but they start to differ at farther damper positions, as seen in Figure 3.1. If the position of the damper is zero implying that there is no damper on the conductor, the maximum relative conductor values are essentially equal. On the other hand, Energy Balance Method estimates higher maximum displacement values when there is a damper on the conductor since it excludes the effects of the damper mass and the conductor flexural rigidity. The maximum relative conductor displacements become zero when the position of the damper reaches a specific value. At these points, the sum of dissipated power by the damper and the conductor becomes larger than the input wind power, which makes the conductor overdamped. Since both Energy Balance Method and Force Based Method are developed on the basis of steady-state monofrequent aeolian vibrations, they cannot distinguish the transient phase of conductor motion. In the field, an overdamped conductor gives responses to the wind-induced forces since the transmission of the wind energy into the damper requires some time [12].

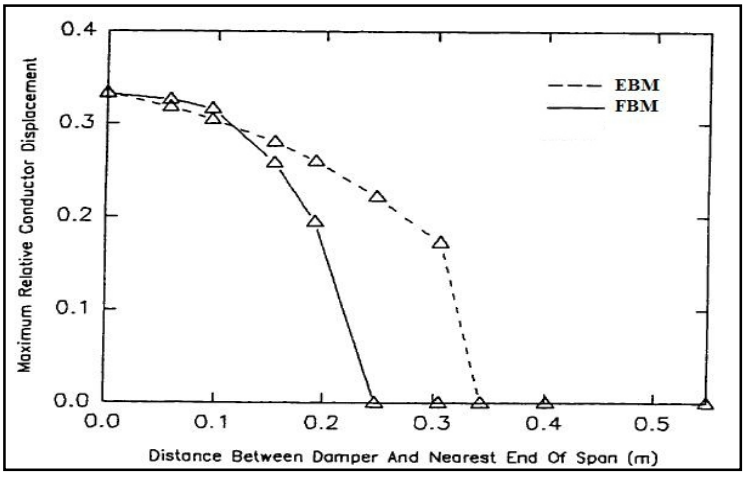

Figure 3.1 Comparison of EBM and FBM by the maximum relative conductor displacements with the damper position for a vibration frequency of 13.9 Hz [12]

Given the above comparative discussion of these two methods, Energy Balance Method is mostly in the safe side. Moreover, Energy Balance Method is the one that is accepted and commonly used by international standards of overhead transmission lines. Hence, Energy Balance Method is utilized in this thesis and it is discussed in more detail in the next subsection.

3.2 Energy Balance Method

As briefly mentioned in the previous subsection, Energy Balance Method is based on a non-linear algebraic equation of power balance among the power of aerodynamic forces brought into the system by the wind, the power dissipated by the conductor due to conductor's self-damping and the power dissipated by the vibration damper.

$$P_{wind}\left(A/D\right) = P_{cond.}\left(A/D\right) + P_{damp.}\left(A/D\right) \tag{3.1}$$

where $P_{wind}\left(A/D\right)$ is the power brought into the system by the wind, $P_{cond.}\left(A/D\right)$ is the power dissipated by the conductor and $P_{damp.}\left(A/D\right)$ is the dissipated power by the vibration damper. Energy Balance Method is based on the frequency domain with these assumptions [12]:

- The flexural rigidity of the conductor is ignored.
- The conductor tension and mass are uniform across the span.
- The conductor is clamped in a horizontal position at each end of the span.
- The suspension clamps are at the same elevation.
- A steady, uniform and horizontal wind flow is considered.
- The conductor vibrates in a standing wave and in the vertical direction.
- The conductor is composed of infinitesimal rigid cylinders which absorb wind power according to their displacement amplitudes.

Moreover, Energy Balance Method has some limitations as briefly mentioned in the previous subsection that it does not account for;

- travelling-wave effects
- contributions from other modes of vibration
- conductor flexural rigidity
- damper mass

In the field, zero motion points cannot exist on the conductor due to the effects of travelling-wave which is the transmission of the mechanical energy along the conductor and this concept constitutes the basis of the Inverse Standing Wave Test method as previously mentioned in the subsection 2.5.2. In a continuous system, all of the natural modes are excited to some degree when the system is forced at a single frequency. However, Energy Balance Method assumes that there is only a single mode at steady state which is the mode corresponding to the shedding frequency of vortices. In order to estimate the bending stresses near the span ends, displacement amplitudes in that region are used and these amplitudes can be affected by the flexural rigidity of the conductor. Finally, the damper mass can change the natural modes and mode shapes of the conductor which can affect the total power dissipation by the conductor and the damper [12].

3.2.1 Power Brought into the System by the Wind

The shedding frequency of vortices generated by the wind is [12];

$$f_{vs} = St\frac{V}{D} \tag{3.2}$$

where f_{vs} is the vortex-shedding frequency $[Hz]$, V is velocity of the wind $[m/s]$ and D is conductor diameter $[m]$. St is the Strouhal number which is generally taken

as 0.185, as seen in Figure 3.2. The Strouhal number indicates a measure of the ratio of inertial forces due to the unsteadiness of the flow or local acceleration to the inertial forces due to changes in velocity from one point to another in the flow field [28]. The range of the Strouhal number is 0.18 to 0.22 for transmission lines in the smooth wind flow of 2 to 15 *mph* (1 to 7 *m/s*) and Strouhal number has a relation with Reynolds number, as seen in Figures 3.3 and 3.4.

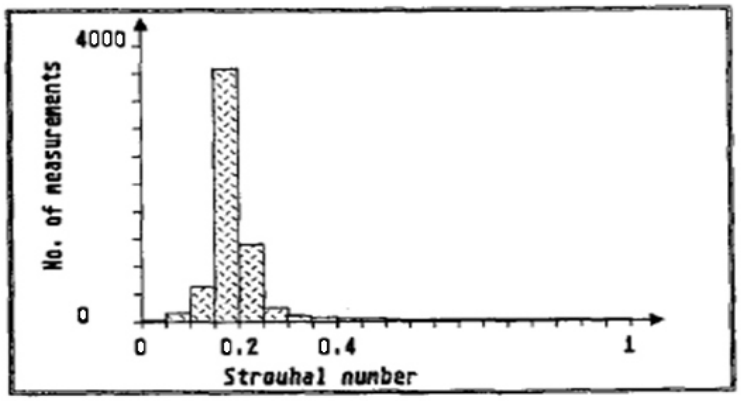

Figure 3.2 Statistical values for the Strouhal number [29]

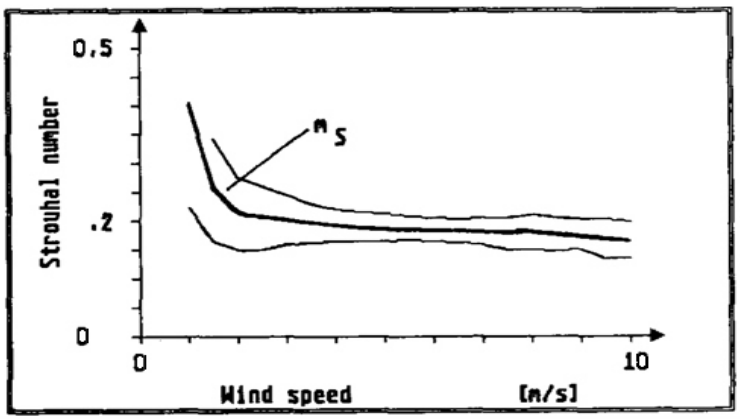

Figure 3.3 Wind Speed Distribution for the Strouhal number [29]

$$Re = \frac{\rho V D}{\mu} \tag{3.3}$$

where Re is the Reynolds number, ρ is the density of the fluid $\left[kg/m^3\right]$ and μ is the dynamic viscosity of the fluid $\left[kg/m.s\right]$.

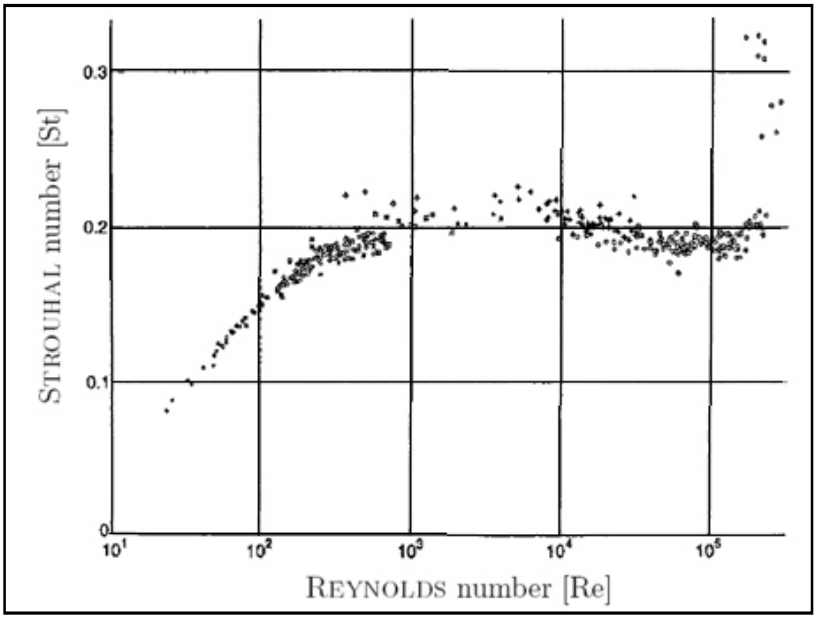

Figure 3.4 Variation of the Strouhal number with the Reynolds number for the flow around cylinders [30]

If f_n is the natural frequency of the cylinder $\left[Hz\right]$, during the lock-in phenomenon [12];

$$f_n = f_{vs} = f \tag{3.4}$$

where f is the lock-in frequency $\left[Hz\right]$ and aerodynamic lift force $\left[N\right]$ on the cylinder varies harmonically that [12];

$$F_a(t) = F_L \sin(wt + \theta) = F_L \sin(2\pi ft + \theta) \tag{3.5}$$

$$w = 2\pi f \tag{3.6}$$

where F_L is the magnitude of lift force $[N]$, w is vibration frequency $[rad/s]$, t is time $[s]$ and θ is the phase angle $[rad]$ between the aerodynamic lift force $F_a(t)$ and the transverse displacement of the cylinder $z(t)$. The transverse displacement $[m]$ of the cylinder (conductor) varies harmonically that [12];

$$z(t) = A\sin(wt) = A\sin(2\pi ft) \tag{3.7}$$

where A is the vertical displacement amplitude (single vibration amplitude) of the cylinder $[m]$. Wind energy $[J]$ for the cylinder is [12];

$$E_{wind} = \int_0^{\frac{1}{f}} F_a(t)\frac{dz(t)}{dt}dt = \pi F_L A\sin\theta \tag{3.8}$$

where $(1/f)$ is the period of the motion. Power *[W]* for the wind (energy brought into the system per cycle of vibration divided by the period $(1/f)$ of the vibration) is;

$$P_{wind} = fE_{wind} \tag{3.9}$$

$$P_{wind} = f\pi F_L A\sin\theta \tag{3.10}$$

$$F_L = \frac{1}{2}C_L\rho DLV^2 \tag{3.11}$$

where C_L is lift coefficient and L is the span length $[m]$ as illustrated in Figure 3.5. So, the power of the wind becomes;

$$P_{wind} = \frac{\pi}{2} f \ \rho D L V^2 A C_L \sin\theta \tag{3.12}$$

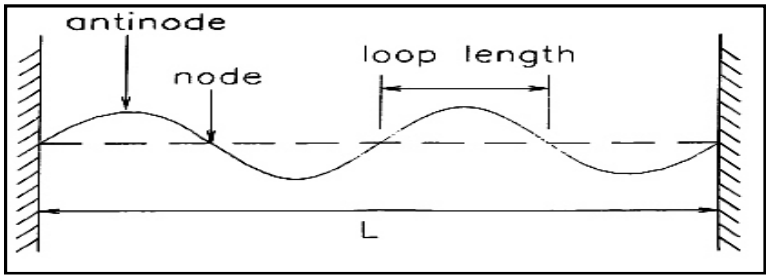

Figure 3.5 Span length, node, anti-node and loop length [12]

If the reduced velocity (dimensionless) is [12];

$$V_r = \frac{V}{f_n D} = \frac{V}{fD} = 1/St \tag{3.13}$$

then the power for the wind with reduced velocity is;

$$P_{wind} = \frac{\pi}{2} f^3 \rho D^3 L V_r^2 A C_L \sin\theta \tag{3.14}$$

and it can be arranged to get both side dimensionless as;

$$\frac{P_{wind}/L}{\rho f^3 D^4} = \frac{\pi}{2} V_r^2 \frac{A}{D} C_L \sin\theta \tag{3.15}$$

It is proved by experiments that V_r, C_L, θ, ρ and (A/D) are all related to each other [12]. Here, ρ can be also taken to the right side of the equation and then the general form of the above equation becomes;

$$\frac{P_{wind}/L}{f^3 D^4} = fnc\left(\frac{A}{D}\right) \tag{3.16}$$

Here, $fnc(A/D)$ is called Reduced Power Function $\left[Wm^{-1}/Hz^3m^4\right]$ and it depends on relative vibration amplitude (A/D). By using this relation, the wind power for all available conductor diameters can be evaluated at all practical values of frequency [31].

3.2.2 Reduced Power Function

Reduced Power Function is an experimental function and the results of wind tunnel experiments of different researchers can be seen from Figure 3.6. There are dispersions among these results because of [31];

- the three-dimensional effects of the wind flow
- the turbulence of the wind tunnel
- the rigidity and roughness of the cylinder
- the effect of the Reynolds' number

In order to reduce the three-dimensional effects, end plates should be used at the extremities of the model to get a two-dimensional flow. In addition, the turbulence in the tunnel and the roughness of the cylinder disturb the smoothness of the flow which reduce the input power of the wind. For the representation of the conductor, rigid or flexible models can be used in the wind tunnel tests and this also differ the test method and the results. Finally, different Reynolds' number produces different

test results as Reynolds' number affects the flow characteristic. Generally, smaller Reynolds' number generates higher input wind power.

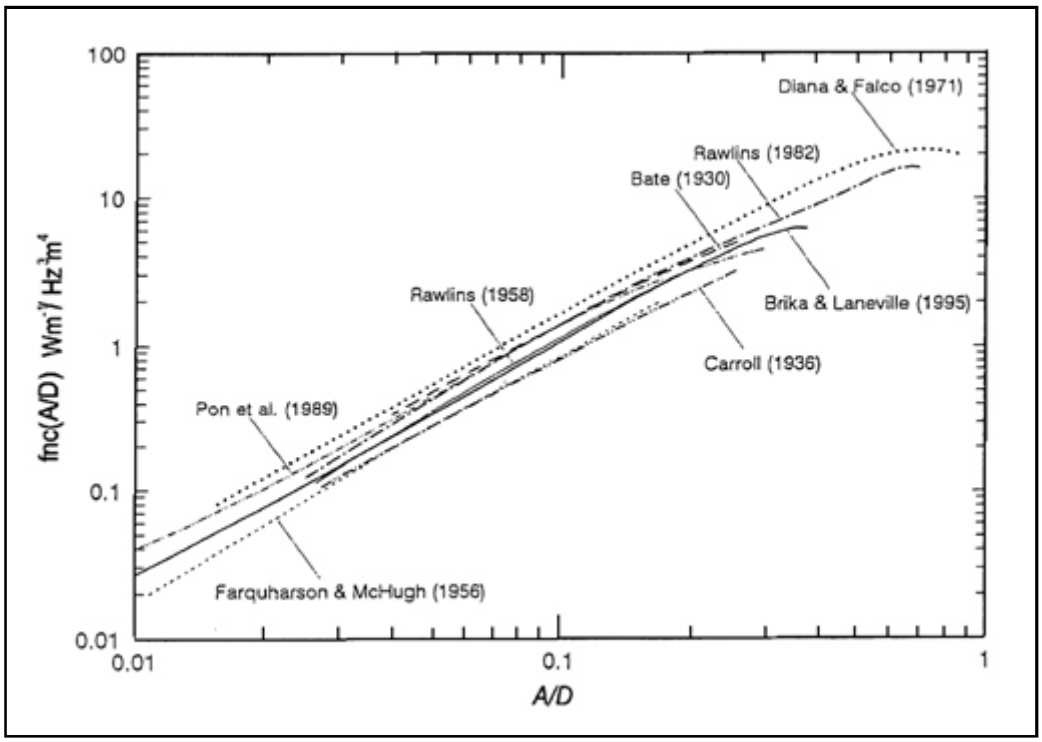

Figure 3.6 Reduced Power Function vs. relative vibration amplitude [31]

For the practical use of the Reduced Power Function, there are polynomials that fit the Figure 3.6 as;

Riegert & Currie (1991) Polynomial [12]

$$fnc\left(\frac{A}{D}\right) = 807.4\left(\frac{A}{D}\right)^{1.953} - 767.6\left(\frac{A}{D}\right)^{2} - 3.2\left(\frac{A}{D}\right)^{3} - 78.2\left(\frac{A}{D}\right)^{4} \tag{3.17}$$

Diana & Falco (1971) Curve [32]

$$fnc\left(\frac{A}{D}\right) = \sum_{n=0}^{9} a_n X^n \tag{3.18}$$

$$X = \log_{10}(2y_0 / D) \tag{3.19}$$

where $a_0 = 1.26575$, $a_1 = 1.69387$, $a_2 = -1.08622$, $a_3 = -12.7859$, $a_4 - 34.162$, $a_5 = -43.7526$, $a_6 = -31.5830$, $a_7 = -13.1900$, $a_8 = -2.96931$ and $a_9 = -0.277980$

Middle Curve between Carroll (1936) and Diana & Falco (1971) [31]

$$fnc\left(\frac{A}{D}\right) = -99.73\left(\frac{A}{D}\right)^3 + 101.62\left(\frac{A}{D}\right)^2 + 0.1627\left(\frac{A}{D}\right) + 0.2256 \tag{3.20}$$

3.2.3 Power Dissipated by the Conductor due to the Self-Damping

The power dissipated by the conductor is calculated as follows [33];

$$P_{cond.}(A) = L\,K\frac{(A/D)^l f^m}{T^n} \tag{3.21}$$

where l, m and n are conductor self-damping exponents, K is the proportionality factor that characterizes the conductor self-damping properties and T is the conductor tension $[N]$. K factor is in the range of 1.5 to 2 for classical conductor material and cross section in the SI system [34] and the related test results of five different laboratories are provided in the Appendix A of [31].

Self-damping exponents obtained by a number of investigators are presented in Table 3.1 with the measurement method, the test span length, the end conditions of the span, the number of conductors and tensions tested. As seen in Table 3.1, there are differences among the conductor self-damping exponential constants which are mainly related to the end conditions of the span. Generally, the use of Power Test (PT) method, which is previously mentioned in subsection 2.5.2, for conductor self-damping measurement on laboratory test spans with rigidly fixed extremities is

inadequate accuracy and the use of pivoted extremities are suggested whenever this method is used [35].

Table 3.1 Conductor self-damping exponents [35]

Investigations	l	m	n	Method	End Cond.	Span length (m)	n° conductors × tensions
Tompkins et al. (1956)	2.3-2.6	5.0-6.0	1.9 (1)	ISWR	N.A.	36	1 × 2
Claren & Diana (1969b)	2.0	4.0	2.5;3.0;1.5	PT	M.B.	46	3 × 3
Seppä (1971), Noiseux (1991)	2.5	5.75	2.8	ISWR	N.A.	36	1 × 8
Rawlins (1983)	2.2	5.4		ISWR	N.A.	36	1 × 1
Lab. A (CIGRE 22.01 1989)	2.0	4.0		PT	M.B.	46	1 × 1
Lab. B (CIGRE 22.01 1989)	2.3	5.2		PT	P.E.	30	1 × 1
Lab. C (CIGRE 22.01 1989)	2.44	5.5		ISWR	N.A.	36	1 × 1
Kraus & Hagedorn (1991)	2.47	5.38	2.80	PT	P.E.	30	1 × ?
Noiseux (1991) (2)	2.44	5.63	2.76	ISWR	N.A.	63	7 × 4
Tavano (1988)	1.9-2.3	3.8-4.2		PT	M.B.	92	4 × 1
Möcks & Schmidt (1989)	2.45	5.38	2.4	PT	P.E.	30	16 x 3
Mechanical Laboratory Politecnico di Milano (2000)	2.43	5.5	2	ISWR	P.E.	46	4 × 2

ISWR: Inverse Standing Wave Method
PT: Power Method
N.A.: Non applicable
M.B.: Massive block
P.E.: Pivoted Extremity
(1): extrapolated
(2): Data corrected for aerodynamic damping

3.2.4 Power Dissipated by the Stockbridge Damper

The dissipated power by the vibration damper is calculated as follows [33];

$$P_{damp.} = 0.25 T c_w k_w^2 \frac{1-(h^2+g^2)}{1+(h^2+g^2)} D^2 \left(\frac{A}{D}\right)^2 \tag{3.22}$$

where c_w is the wave velocity $[m/s]$ and k_w is the wave number $[rad/m]$. They are calculated as;

$$k_w = 2\pi f \sqrt{\frac{m_L}{T}} \tag{3.23}$$

$$c_w = \sqrt{\frac{T}{m_L}} \tag{3.24}$$

where m_L is the conductor mass per unit length $[kg/m]$. Also, the constants h, g and γ are calculated as;

$$h = -\frac{\sin^2(k_w l_1)[\sin(2k_w l_1) + 2\gamma \sin\alpha]}{\sin^2(k_w l_1) + \gamma^2 + 2\gamma \sin(k_w l_1)\sin(k_w l_1 + \alpha)} \tag{3.25}$$

$$g = \frac{\sin^2(k_w l_1)\cos(2k_w l_1) + \gamma^2 + \gamma \sin(2k_w l_1)\sin\alpha}{\sin^2(k_w l_1) + \gamma^2 + 2\gamma \sin(k_w l_1)\sin(k_w l_1 + \alpha)} \tag{3.26}$$

$$\gamma = \frac{T}{Z\ c_w} \tag{3.27}$$

where l_1 is the distance between the damper and the suspension clamp $[m]$, α is the phase angle between force and velocity at the shaker test $[rad]$ and Z is the damper impedance at the shaker test (absolute ratio between force and velocity) $[N.s/m]$. If the damper is placed on a nodal position of the conductor, $(h^2 + g^2)$ approaches to 1 and the equation (3.22) yields zero that there is no power dissipation by the damper.

3.2.5 Bending Strain and Stress

Maximum bending strain of the conductor *[m/m]* at the suspension clamp, which is based on the outer-layer wire strand, is calculated by using the peak-to-peak displacement amplitude of the conductor as [6], [25];

$$\varepsilon_b = \frac{p^2 d_o}{4(e^{-px_b} - 1 + px_b)} Y_b \tag{3.28}$$

$$p = \sqrt{T / EI} \tag{3.29}$$

where p is the bending stiffness parameter $\left[m^{-1}\right]$, d_o is the diameter of outer-layer strand $[m]$, x_b is the distance from the last point of conductor contact with clamp to the measurement point $[m]$ which is generally 89 *mm* as mentioned previously in the subsection 2.6, Y_b is the peak-to-peak displacement amplitude of the conductor $[m]$ relative to the clamp at x_b $[m]$ as illustrated in Figure 3.8, EI is the sum of flexural rigidities of individual wire strands in the conductor $\left[N.m^2\right]$ and calculated as;

$$EI = \frac{\pi}{64} \sum_{i=1}^{j} n_i d_i^4 E_i \tag{3.30}$$

where j is the number of layers in the conductor, n_i is the number of the wire strands in the ith layer, d_i is the diameter of the wire strands in the ith layer and E_i is the Young's modulus of elasticity of the material for the wire strands in the ith layer. In Figure 3.7, a representation of a three-layer conductor is given.

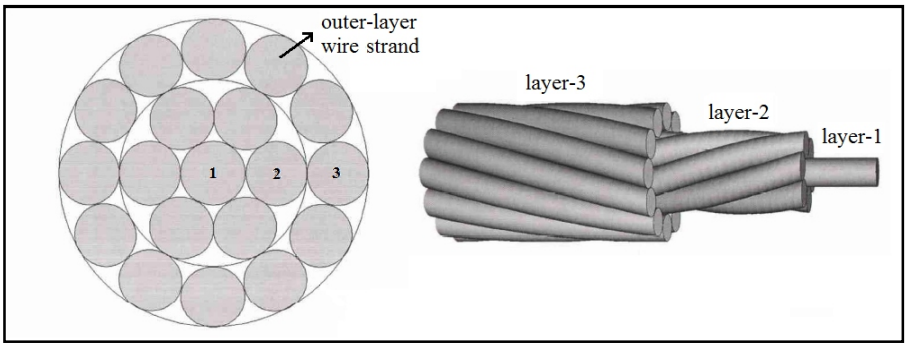

Figure 3.7 Representation of a three-layer conductor adopted from [36]

On the other hand, maximum bending strain of the conductor at the suspension clamp can also be calculated by using the maximum vibration amplitude of the conductor which is also illustrated in Figure 3.8 [26], [37];

$$\varepsilon_b = \pi d_o \sqrt{\frac{m_L}{EI}} fA \tag{3.31}$$

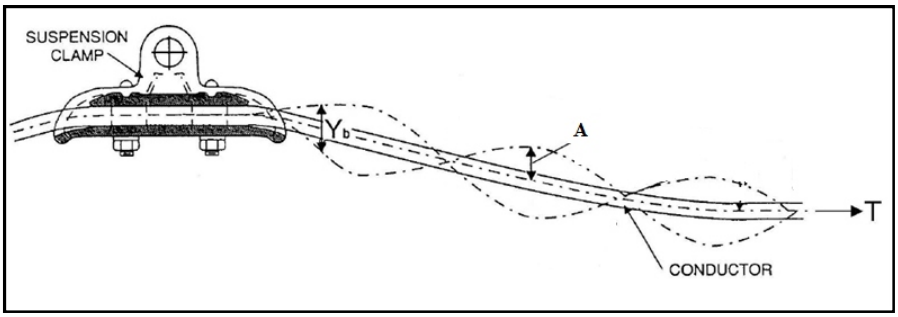

Figure 3.8 Representation of bending amplitude Y_b and the displacement amplitude A of the conductor [26]

By using the equation (3.23) or (3.26), maximum bending stress $[Pa]$ can be calculated from the maximum bending strain as;

$$\sigma_b = E_o \varepsilon_b \tag{3.32}$$

where E_o is the Young's Modulus for the outer-layer strand material $[Pa]$.

3.2.6 Displacement of the Conductor

Generally, a single conductor is modeled as a taut string and the displacement of the conductor *[m]* along the span is [38];

$$y = A\sin(\frac{2\pi}{\lambda}x) = A\sin(\frac{r\pi}{L}x) \tag{3.33}$$

where x is the distance from the suspension clamp $[m]$, r is the mode number and λ is the wave length $[m]$ which is;

$$\lambda = \frac{1}{f}\sqrt{\frac{T}{m_L}} \tag{3.34}$$

CHAPTER 4

DEVELOPMENT OF THE SOFTWARE

In this chapter, the conceptual and the detailed design of the software are discussed together with the inputs and the outputs. The interface of the software is presented in more detail with the capabilities of the software. The validation step of the software is completed with and without damper cases by utilizing existing field tests. In addition to the field tests, a number of case studies are employed to measure the accuracy of the software.

4.1 Conceptual Design

In this thesis, it is aimed to evaluate the effectiveness of the Stockbridge dampers on the overhead transmission lines by Energy Balance Method based software with a user friendly interface. For this purpose, MATLAB is chosen to develop the software since it provides various advantages including ready to use functions, capability of reading and writing large data files with variety of formats and easy to built up an interface by GUI (Graphical User Interface).

As mentioned previously, the software is based on the energy balance among the energy introduced by the wind, the energy dissipated by the conductor due to the conductor's self-damping and the energy dissipated by the vibration damper. In this concept, there are inputs such as environmental conditions, conductor properties and the damper characteristic parameters. After the energy balance is achieved as illustrated in equation (3.35), the maximum steady state vertical vibration amplitude

is computed for the conductor. In this equation, Riegert & Currie (1991) polynomial is used for the wind power estimation and the computation of the maximum vibration amplitude is based on the trial and error method. As mentioned previously in subsection 2.2, the maximum vibration amplitude is generally equal to the conductor diameter when the most serious aeolian vibrations occur and therefore the maximum vibration amplitude computation begins with the 1.5 times of the conductor diameter. The initial target error is in the range of ±0.001 *mm* and it increases up to ±0.1 *mm* during the iterations. In this computation, the biggest value is used when there are multiple solutions and this attitude keeps the user in the safety side. Other numerical methods can be also used instead of the trial and error method to compute the roots of the polynomial.

$$f^3 D^4 L\left[807.4\left(A/D\right)^{1.953} - 767.6\left(A/D\right)^2 - 3.2\left(A/D\right)^3 - 78.2\left(A/D\right)^4\right] = L\,K\frac{(A/D)^l f^m}{T^n} + 0.25 T c_w k_w^2 \frac{1-(h^2+g^2)}{1+(h^2+g^2)} D^2 (A/D)^2 \qquad (4.1)$$

In addition, related maximum bending strains and stresses of the conductor at the suspension clamp are also calculated to evaluate the performance of the Stockbridge damper. Finally, tables and plots related to the computed values are utilized to compare the analytical results with the field test results. The conceptual design schematic, which illustrates the calculation and validation steps, is given in Figure 4.1.

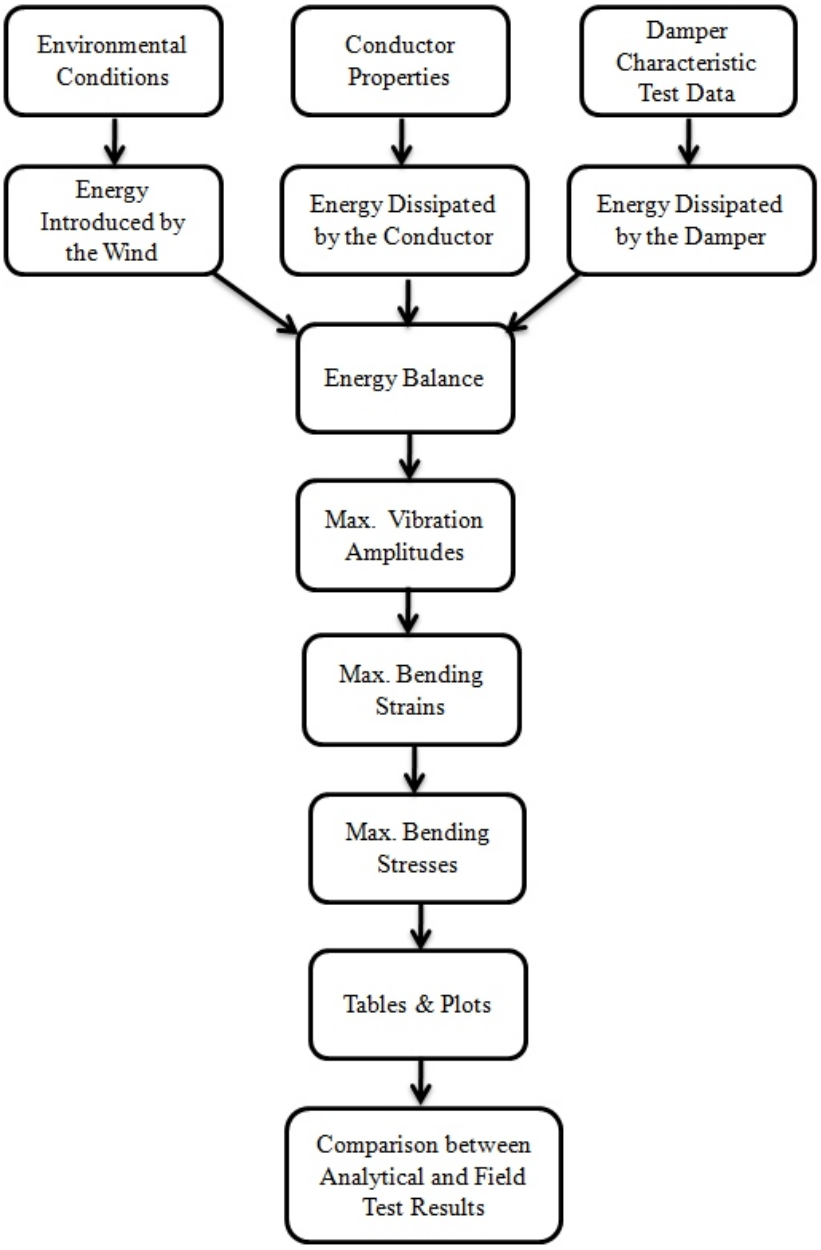

Figure 4.1 Schematic of the conceptual design

4.2 Detailed Design

Being in line with the conceptual design discussed above, the software is developed by using MATLAB and a user friendly interface is also built up by using GUI. There

are two computation options in the software to perform the above mentioned computations. The first calculation option is introducing the characteristic test data file of the damper which is prepared by EXCEL to the software. In this input data file, there are force [N], velocity [m/s] and phase angle [$^\circ$] values with the related frequencies [Hz] measured during the Stockbridge damper characteristic test which is performed as stated in the international standard IEC 61897 [5]. Sample input data related to the Stockbridge damper characteristic test for the software is given in Table 4.1 and a view of the interface for the first calculation option is provided in Figure 4.2. The details of this test are discussed in Chapter 6.

Table 4.1 Sample input data related to the Stockbridge damper characteristic test

Frequency [Hz]	V_{clamp} *[m/s]*	$F_{damp.}$ *[N]*	*Phase Angle [°]*
5.0	0.100	24.1	90.0
7.0	0.100	45.4	8.0
10.0	0.100	28.8	15.0
12.0	0.100	25.3	35.0
15.0	0.100	33.3	40.0
18.0	0.100	60.5	10.0
20.0	0.100	54.4	2.0
25.0	0.100	37.1	3.0
30.0	0.100	26.1	4.0
35.0	0.100	23.3	15.0
40.0	0.100	20.4	30.0

On the other hand, these test data values can also be introduced to make the computation for a specific wind velocity [m/s] in the second calculation option of the software. At this time, the lock-in frequency has to be calculated by entering the target wind velocity [m/s] into the software. A view of the interface for the second calculation option is given in Figure 4.3.

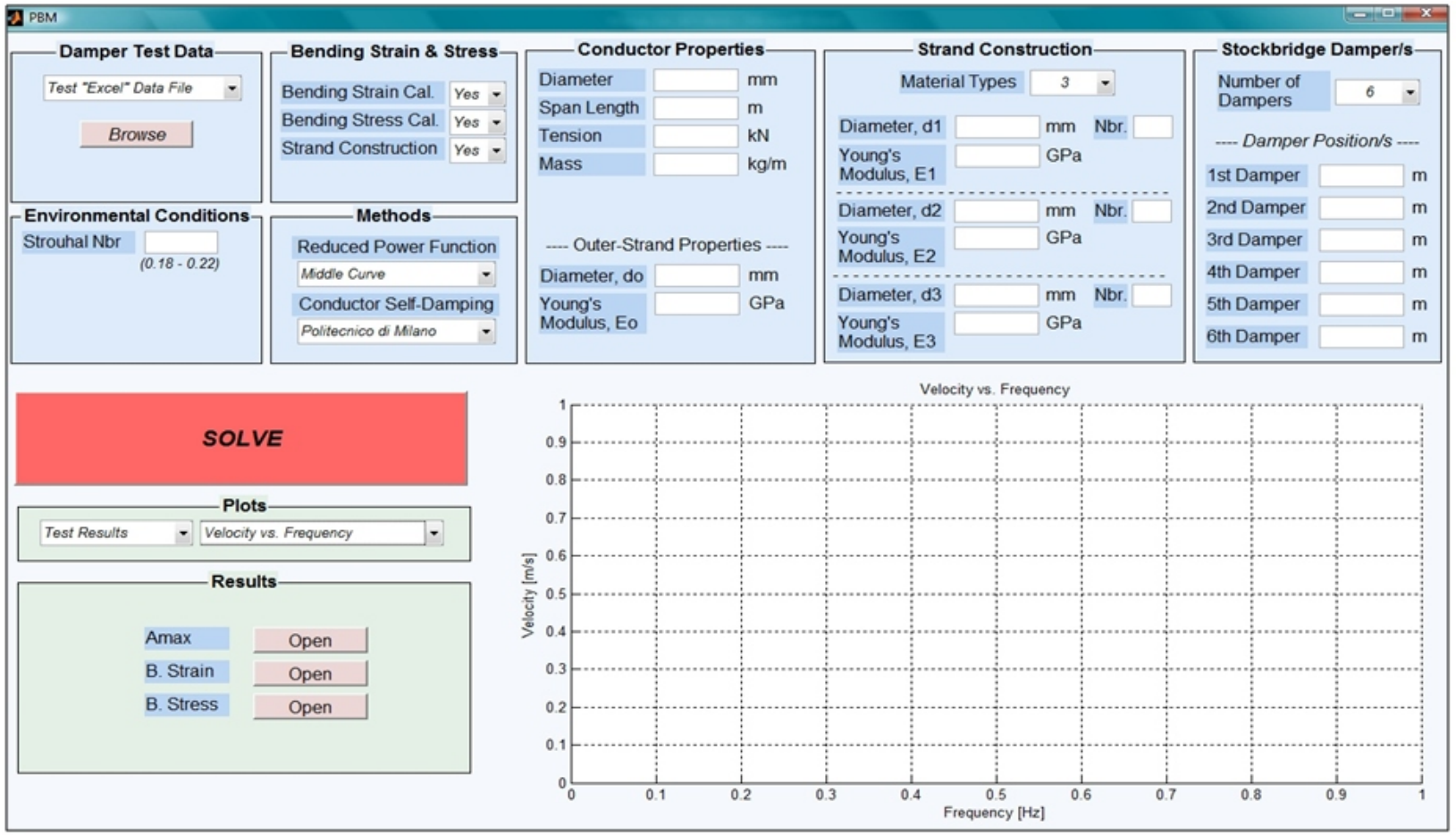

Figure 4.2 Interface of the software for the multiple calculations with a test data file of the damper

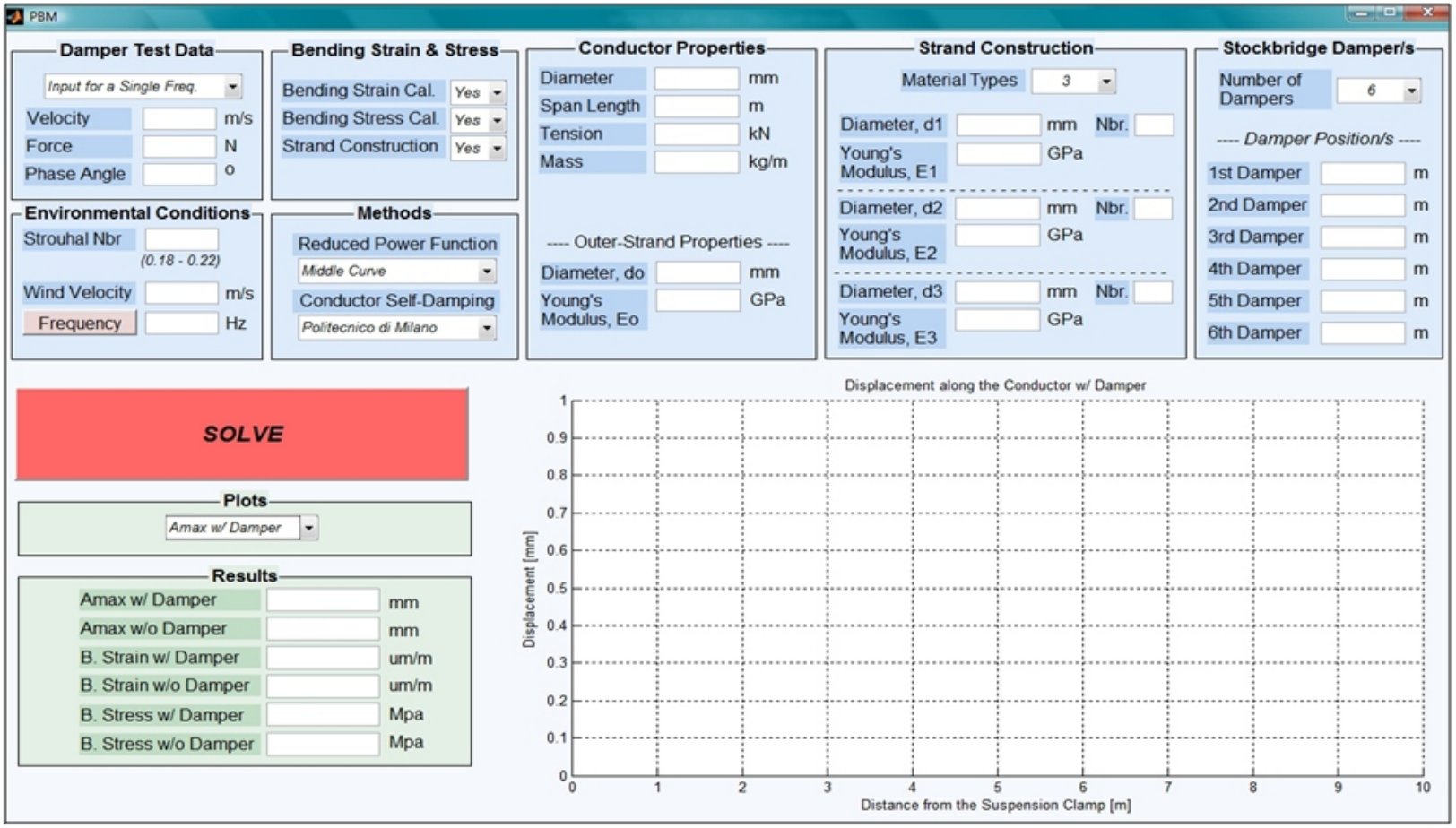

Figure 4.3 Interface of the software for specific wind velocity calculations with the related test data of the damper

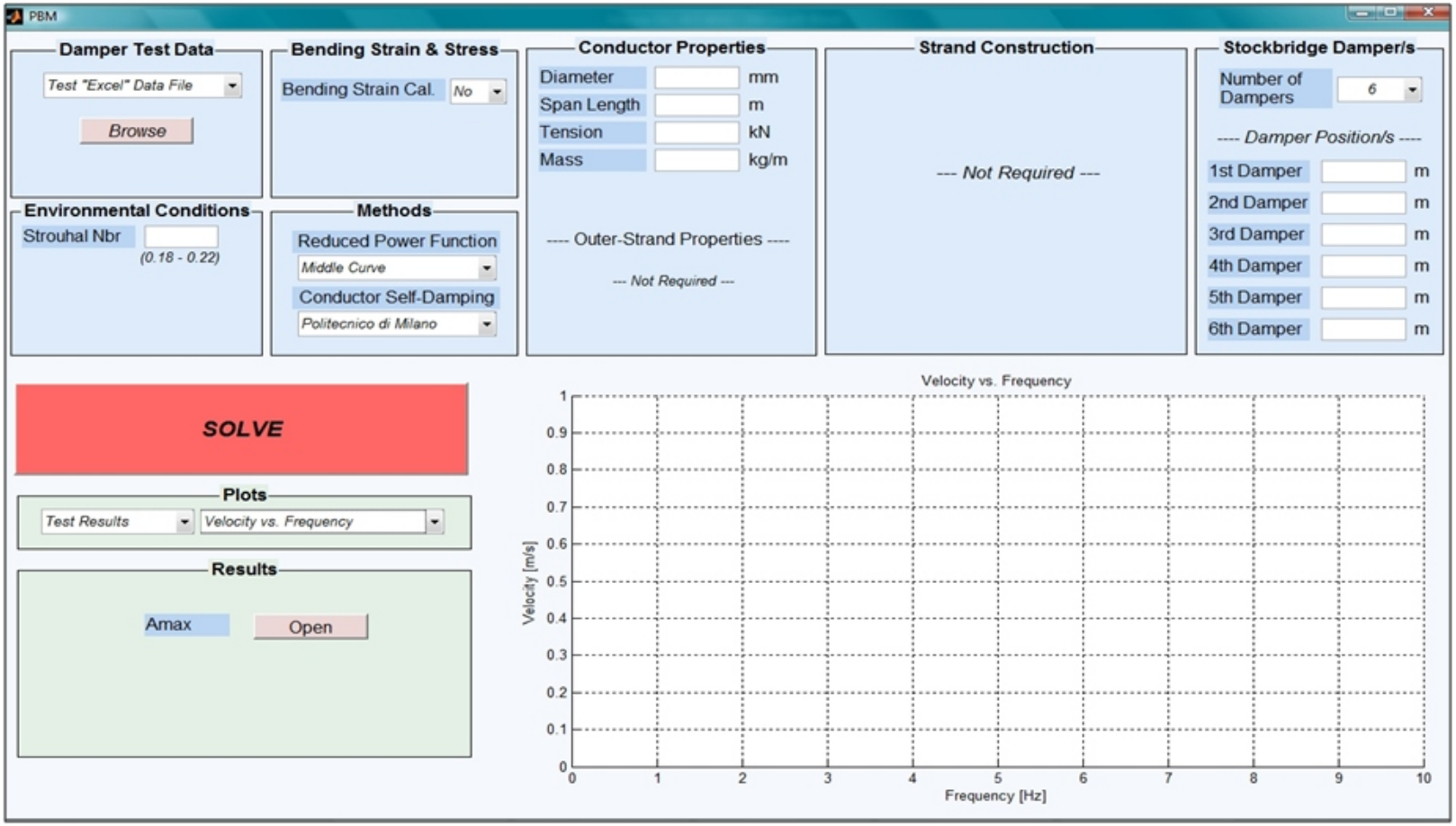

Figure 4.4 Interface of the software for the maximum vibration amplitude calculations with a test data file of the damper

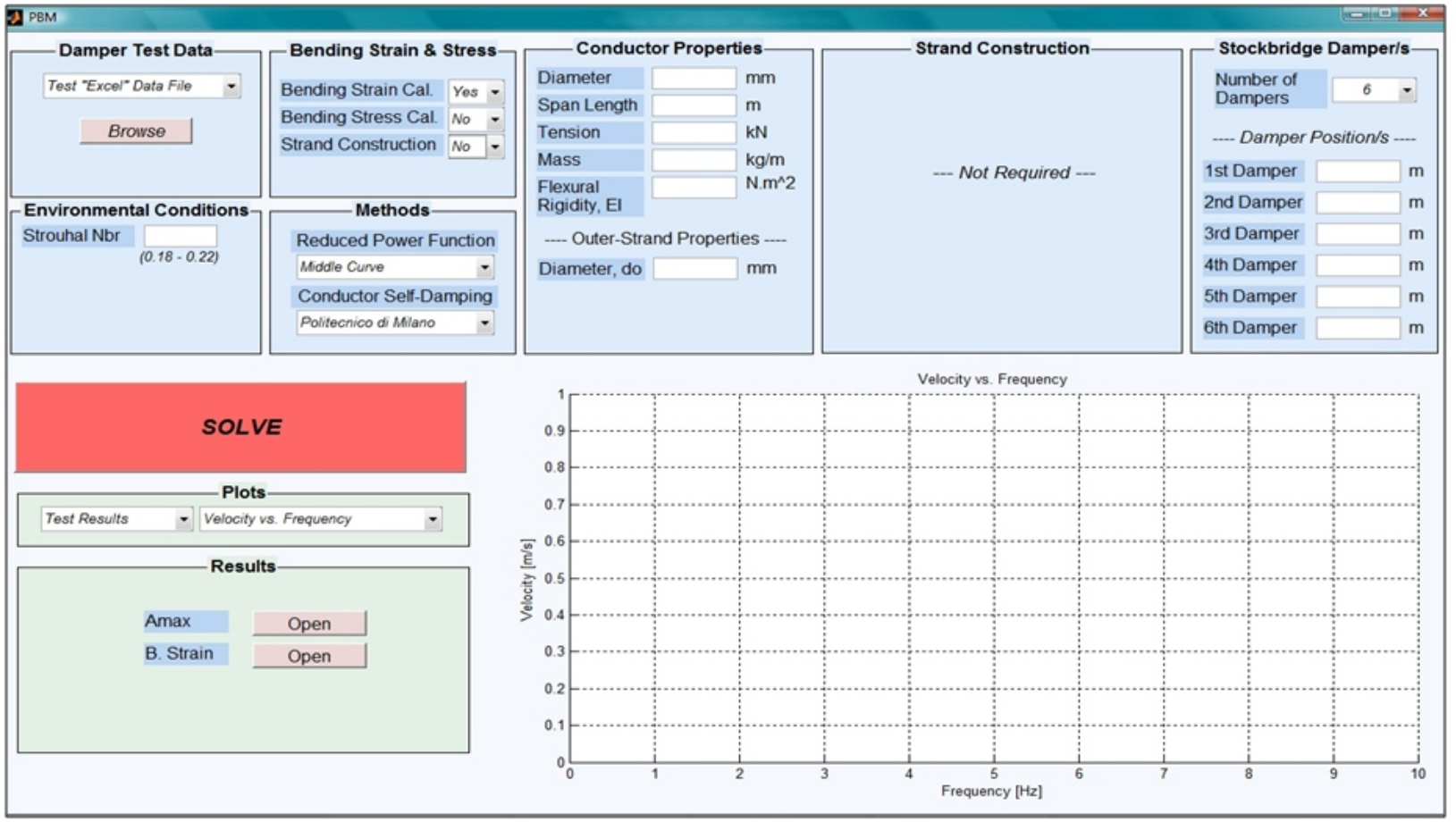

Figure 4.5 Interface of the software for the maximum bending strain calculations without the strand construction part

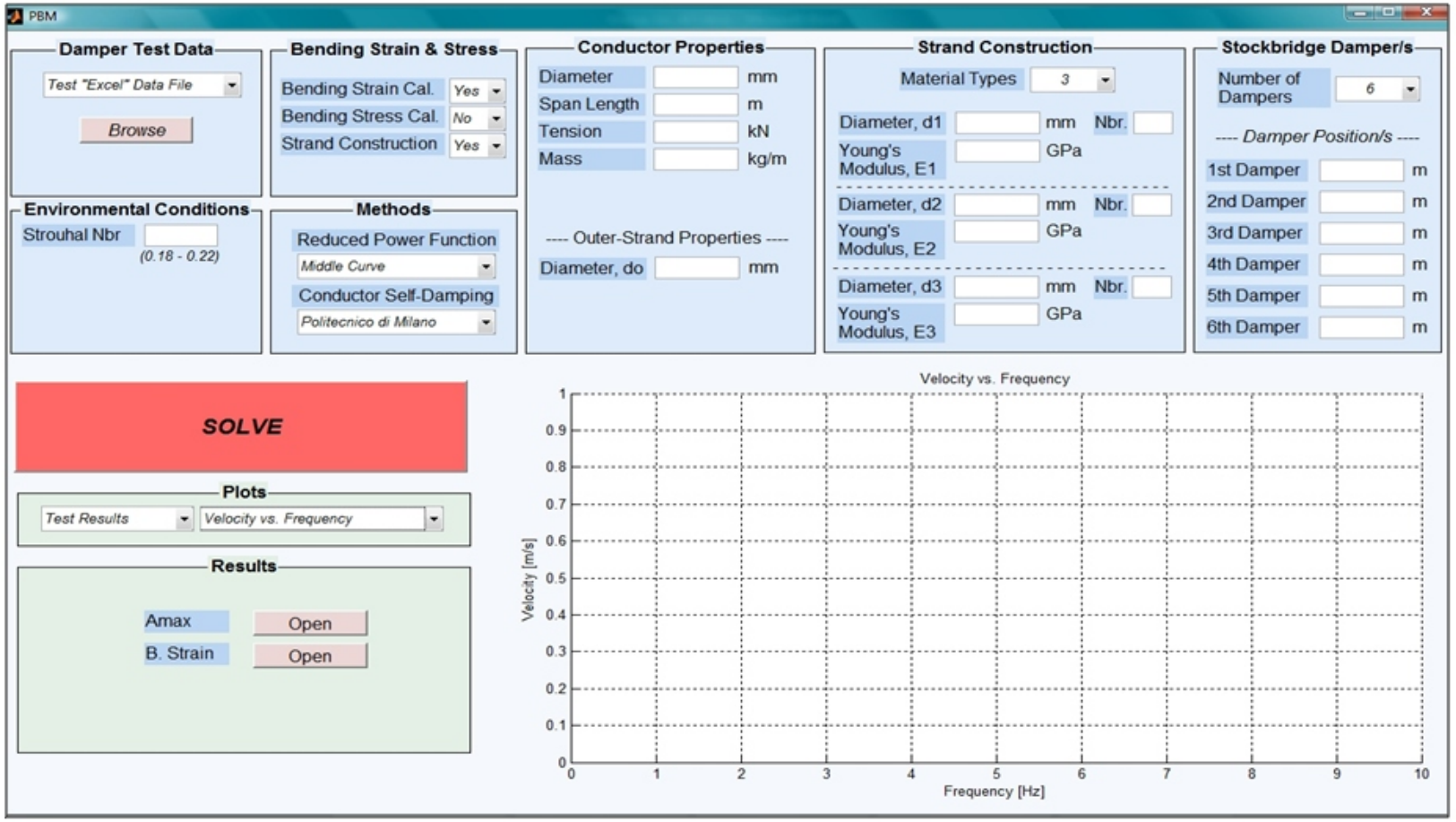

Figure 4.6 Interface of the software for the maximum bending strain calculations with the strand construction part

From now on unless otherwise stated, all discussions are valid for both calculation options of the software. Strouhal number is taken as 0.185 in this study but can be altered in the range of 0.18 to 0.22 as discussed previously in the subsection 3.2.1. Maximum vibration amplitudes of the conductor with and without damper are always calculated although maximum bending strains and stresses of the conductor at the suspension clamp with and without damper are elective for the user as seen in Figures 4.2, 4.4 and 4.5. Flexural rigidity of the conductor $[Nm^2]$ and the outer-layer strand diameter $[mm]$ has to be entered if the maximum bending strains are demanded as illustrated in Figure 4.5. Besides, the strand construction is an alternative of the software for the required flexural rigidity of the conductor and can be used by introducing the diameters $[mm]$, Young's modulus of the materials $[GPa]$ and the number of the individual strands. The strand construction part of the software allows the user to enter up to three material types with unlimited number of strands as seen in Figure 4.2. In the maximum stress calculations, Young's modulus of the outer-layer strand material $[GPa]$ is also required in addition to the above inputs as illustrated in Figure 4.2.

No matter which computation is chosen, the diameter $[mm]$, span length $[m]$, tension $[kN]$ and mass per unit length $[kg/m]$ of the target conductor should be introduced with the number of dampers used on the conductor and the related damper positions $[m]$. Up to six dampers can be placed on the conductor and their positions should be specified according to one of the suspension clamp of the conductor as seen in Figure 4.2.

Riegert & Currie (1991) polynomial, Diana & Falco (1971) curve and the middle curve introduced previously in subsection 3.2.2 can be chosen as the wind power calculation method. While considering the conductor self-damping properties, Politecnico di Milano (2000), Tomkins (1956) and Claren & Diana (1969) are the alternative exponents which are given previously in Table 3.1.

In the results part of the software, user can reach the calculated values, which are in the range of wind velocities and the frequencies, in an EXCEL file for the first calculation option of the software as seen in Figure 4.2. The computed maximum vibration amplitudes $[mm]$, bending strains $[\mu m/m]$ and the stresses $[MPa]$ of the conductor at the suspension clamp are plotted individually in the plot region. These plots contain the conductor's with and without damper conditions versus the lock-in frequency $[Hz]$ or the wind velocity $[m/s]$. In addition, damper characteristic test result, which are "Velocity vs. Frequency", "Force vs. Frequency", "Phase Angle vs. Frequency", "Mechanical Impedance vs. Frequency" and "Power Dissipation vs. Frequency", are plotted in this region of the software. On the other hand, in the second calculation option of the software, maximum vibration amplitude, bending strain and the stress of the conductor at the suspension clamp are given in the results part since the computation is based on a specific wind velocity. At this time, the displacement of the conductor versus the distance from the suspension clamp plots are available with and without damper conditions in the plot region as illustrated in Figure 4.3.

4.3 Validation of the Software

As mentioned previously, an analytical method can be used to analyze the effectiveness of the Stockbridge dampers but it should be validated against the laboratory results or the field test results [5]. In this study, existing field tests are used for the validation of the software. In the first validation step, two existing field tests are employed to evaluate the computed maximum vibration amplitudes of the conductors without dampers.

The duration of the first field test is eight weeks and ACAR 1300 conductor is the target of the aeolian vibrations. The conductor properties of ACAR 1300 are given in Table 4.2. In this computation, the middle curve introduced previously in subsection

3.2.2 is used for the estimation of the wind power and the self damping exponents of Tomkins (1956) are used for the estimation of the dissipated power by the conductor.

Table 4.2 ACAR 1300 conductor properties [31]

ACAR 1300	
Composition	19 Al / 18 Alloy
Diameter [mm]	33.33
Mass [kg/m]	1.816
Ultimate Tension [kN]	145.5
Every day Tension [kN]	29
Span Length [m]	457

Comparison of the estimated maximum vibration amplitudes for the ACAR 1300 conductor with the field test results reveals that they follow almost the same pattern as seen in Figure 4.7. Generally, Energy Balance Method estimates the maximum vibration amplitudes higher than the field and this attitude keeps the user in the safety side.

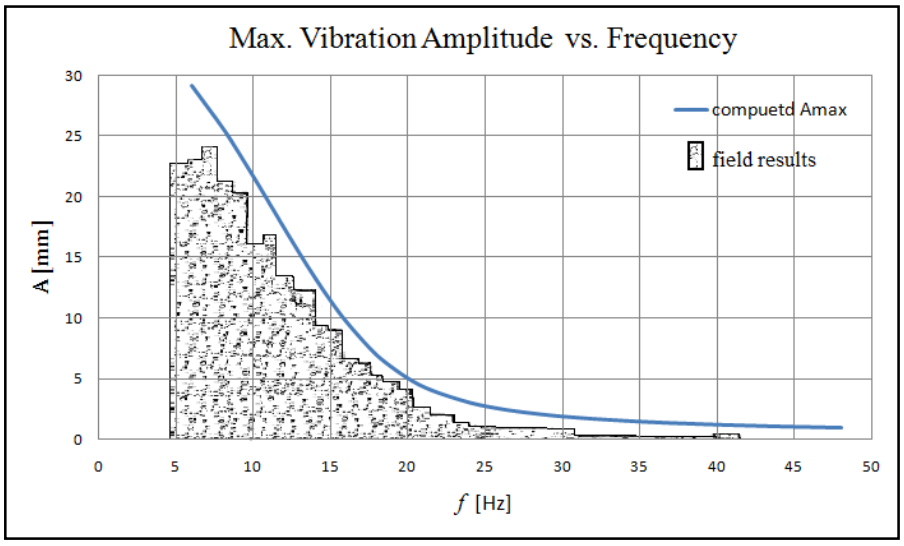

Figure 4.7 Comparison of the computed values with the ACAR 1300 conductor field test results [31]

The duration of the second field test is six weeks and an ACSR type conductor is the target of the aeolian vibrations at this time and the conductor properties are given in Table 4.3. In this computation, Riegert & Currie (1991) polynomial is used for the estimation of the wind power and the self damping exponents of Politecnico di Milano (2000) are used for the estimation of the dissipated power by the conductor.

Table 4.3 ACSR type conductor properties [31]

ACSR Type Conductor	
Composition	54 Al / 19 St
Diameter [mm]	31.5
Mass [kg/m]	1.92
Ultimate Tension [kN]	171.61
Every day Tension [kN]	34.5
Span Length [m]	453

When the computed values for the ACSR type conductor are compared with the field test results, differences appear due to the some missing experimental data however they are still quite close to each other as seen in Figure 4.8. The software computes the maximum vibration amplitudes of the conductor however the vibration levels may not reach their maximum in the field.

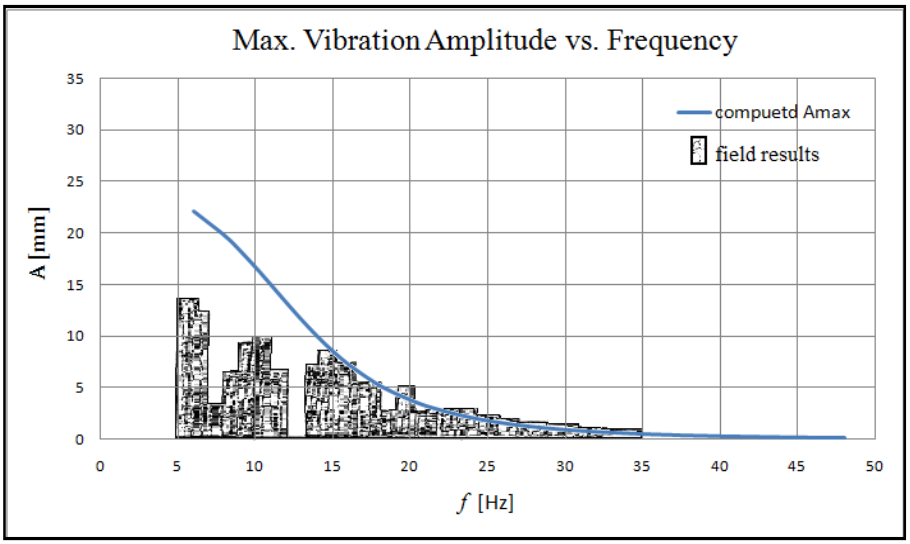

Figure 4.8 Comparison of the computed values with the ACSR type conductor field test results [31]

In the second validation step, field tests of the ACSR 490/65 conductor with and without damper are used to evaluate the estimated maximum stresses of the conductor at the suspension clamp. The conductor properties of ACSR 490/65 are given in Table 4.4.

Table 4.4 ACSR 490/65 conductor properties [39]

ACSR 490/65	
Composition	54 Al / 7 St
Diameter [mm]	30.6
Mass [kg/m]	1.866
Ultimate Tension [kN]	153.1
Every day Tension [kN]	38.3
Span Length [m]	520
E_{al} *[GPa]*	69
E_{st} *[Gpa]*	200
Strand Diameter [mm]	3.4

Two Stockbridge dampers at each suspension clamp are used and placed symmetrically on the conductor with the distance 1.1 *m* to the suspension clamp and within each other. The impedance of the Stockbridge damper is given in Figure 4.9.

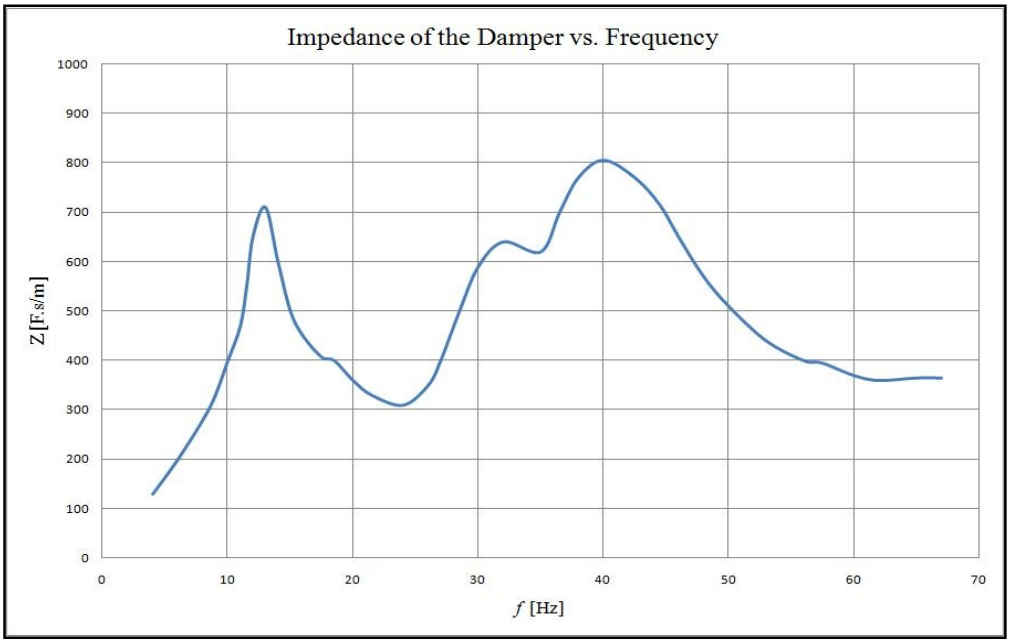

Figure 4.9 Impedance of the Stockbridge damper for the ACSR 490/65 field test [39]

The duration for the measurements without the damper is 41 days and with the damper is 38 days [39]. In this computation, the middle curve is used for the estimation of the wind power and the self damping exponents of Politecnico di Milano (2000) are used for the estimation of the dissipated power by the conductor.

When the estimated maximum stress values of the ACSR 490/65 conductor at the suspension clamp are compared with the field test results with and without dampers, they are close to each other as seen in Figure 4.10. As seen from Figure 4.9, for the impedance of the Stockbridge damper a trough is observed between 20 Hz and 30 Hz, which turns to a peak in Figure 4.10.

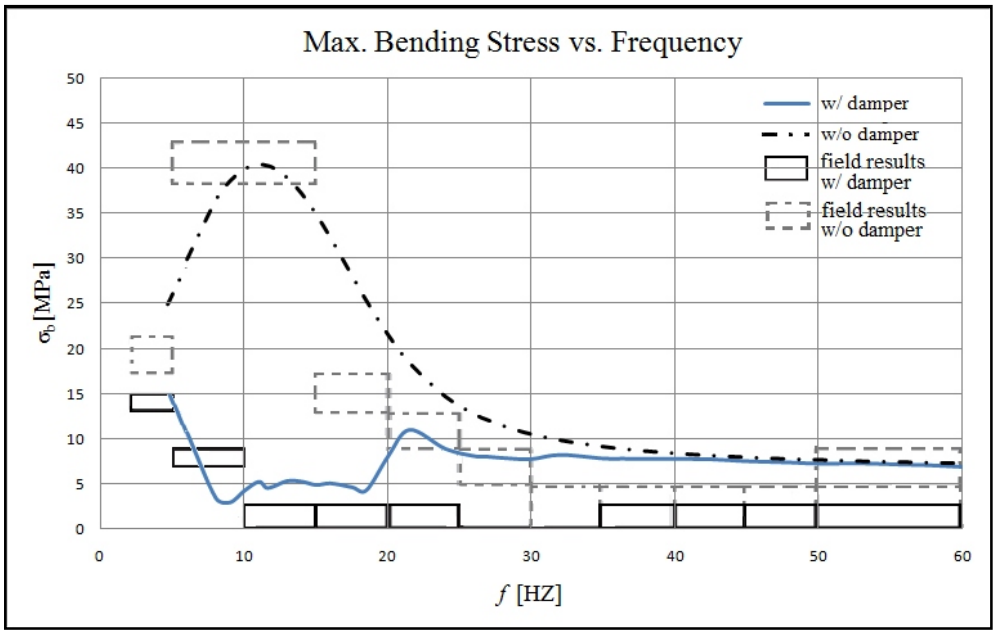

Figure 4.10 Comparison of the computed values with the ACSR 490/65 conductor field test results [39]

4.4 Case Studies

As mentioned previously, there are alternative estimation curves for the wind power and self-damping exponential constants for the dissipated power by the conductor. The software enables user to combine the wind power estimation methods with the self-damping exponential constants and compare them. In this section, the Stockbridge damper characteristic test result given in the international standard IEC 61897 is used for the cases with dampers [5] and the power dissipation curve of the damper is given in Figure 4.11. Two Stockbridge dampers, which are placed symmetrically to the positions of 1.3 *m* at each end of the conductor, are used in the related calculations. The maximum vibration amplitudes and the maximum bending strains of ACSR Cardinal conductor, whose properties are given in Table 4.5, are computed with the following cases;

- Case 1: Riegert & Currie (1991) polynomial and Tomkins (1956) conductor self-damping exponential constants

- Case 2: Diana & Falco (1971) curve and Politecnico di Milano (2000) conductor self-damping exponential constants
- Case 3: Middle curve and Tomkins (1956) conductor self-damping exponential constants
- Case 4: Middle curve and Claren & Diana (1969) conductor self-damping exponential constants

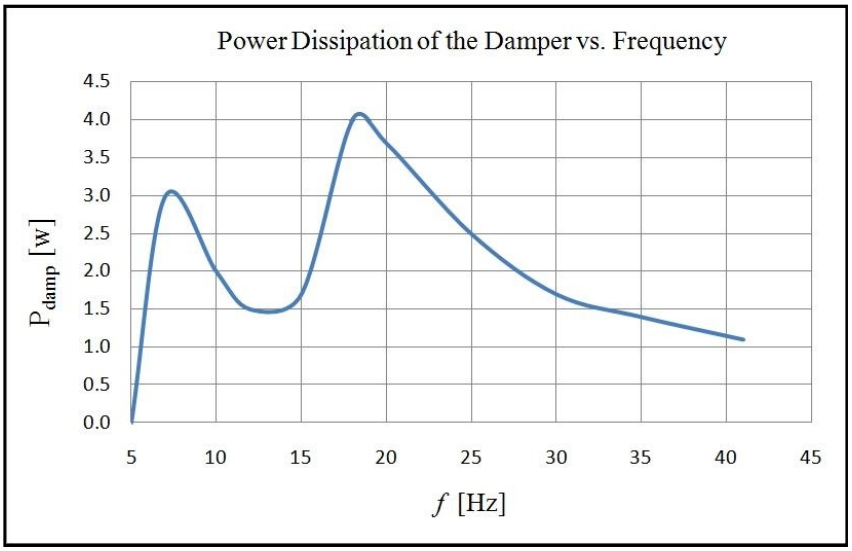

Figure 4.11 Power dissipated by the Stockbridge damper given in IEC 61897 [5]

Table 4.5 ACSR Cardinal Conductor properties [40]

ACSR Cardinal Conductor	
Composition	54 Al / 7 St
Diameter [mm]	30.42
Mass [kg/m]	1.826
Ultimate Tension [kN]	150.4
Every day Tension [kN]	30.1
Span Length [m]	250
Flexural Rigidity [Nm^2]	32.8
Strand Diameter [mm]	3.38

When the estimated maximum vibration values of the ACSR Cardinal conductor without dampers are examined, the first three cases are close to each other but the forth one is differ from them apparently as seen in Figure 4.12. This is an expected result for the Case-4 due to its self-damping exponential constant as mentioned previously in the subsection 3.2.3. From now on, the computation is performed for the first three cases and the computed maximum vibration amplitudes of the conductor with dampers, maximum strains of the conductor at the suspension clamp without and with dampers are illustrated respectively in Figures 4.13, 4.14 and 4.15.

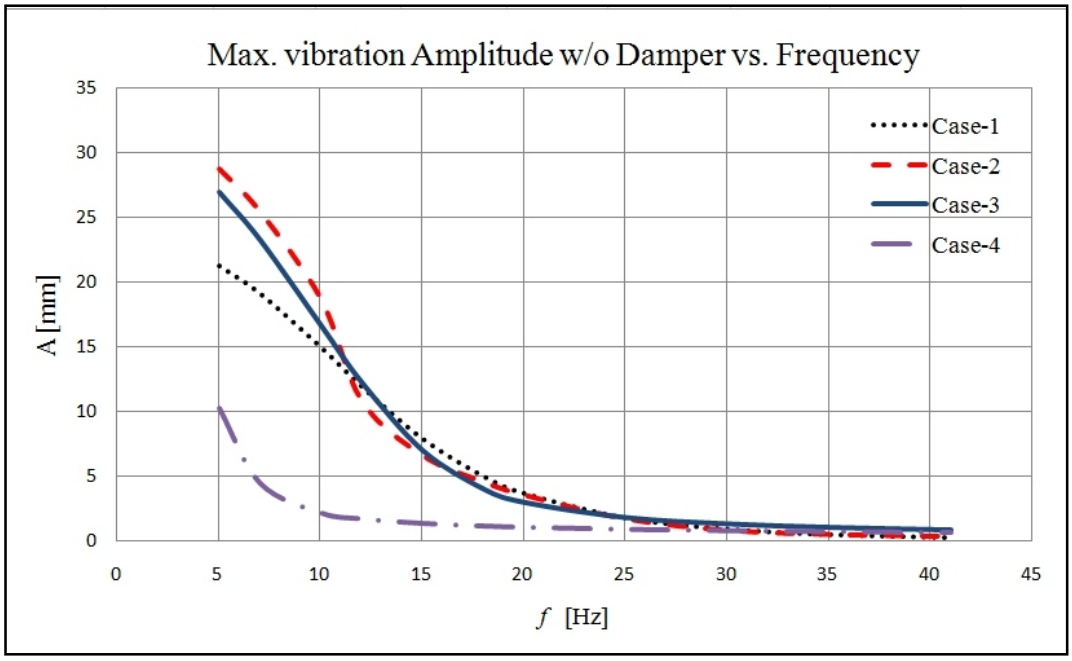

Figure 4.12 Computed max. vibration amplitudes of the conductor without dampers for Case-1, Case-2, Case-3 and Case-4

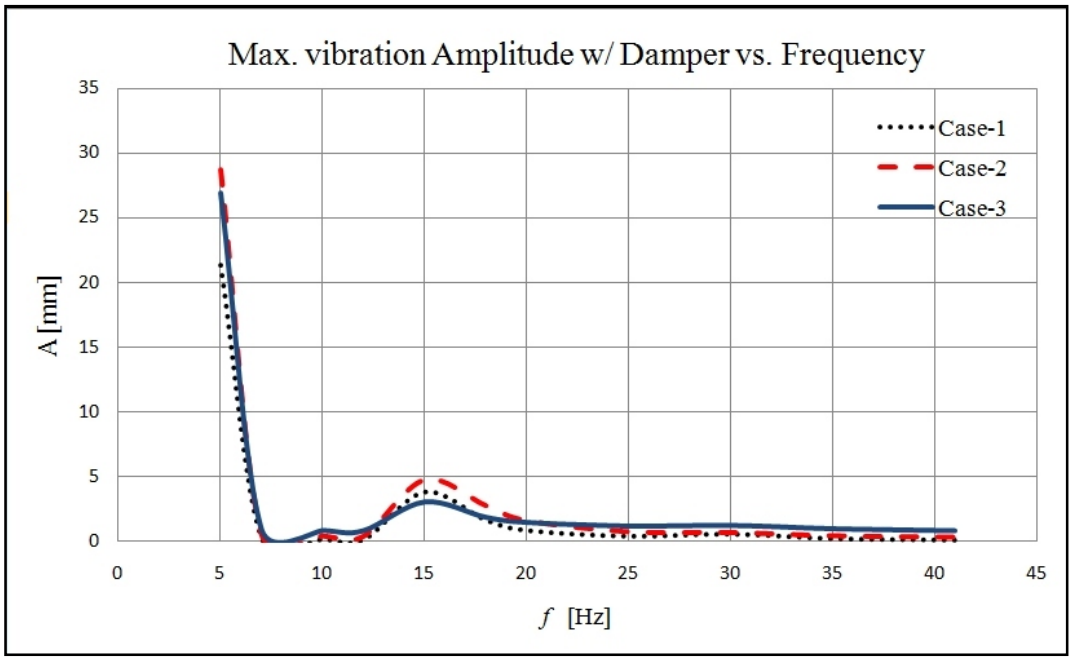

Figure 4.13 Computed max. vibration amplitudes of the conductor with dampers for Case-1, Case-2, Case-3 and Case-4

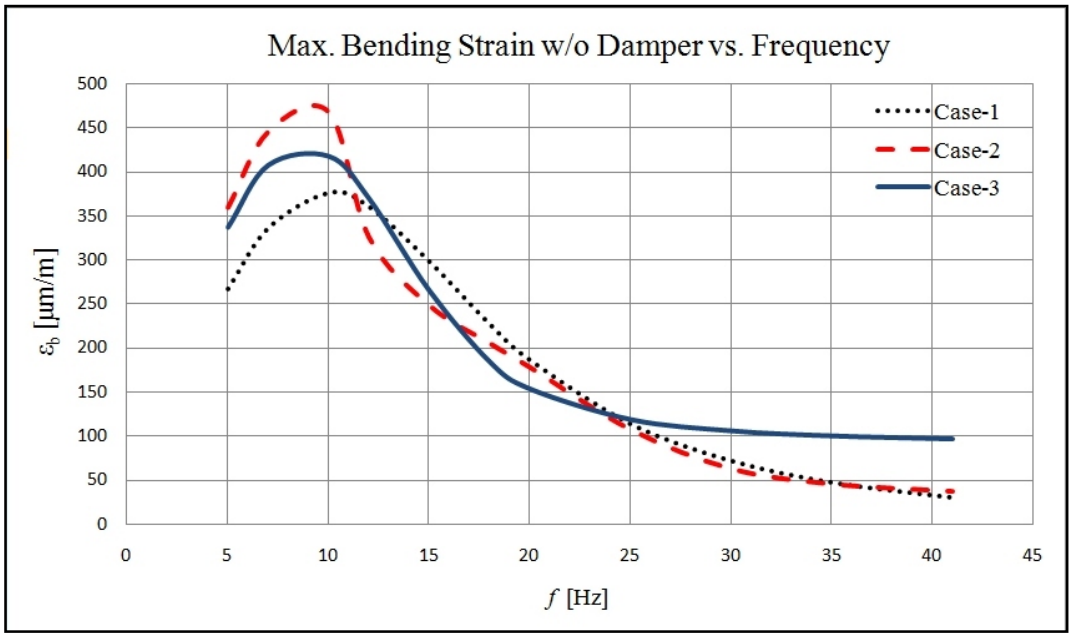

Figure 4.14 Computed max. strains of the conductor at the suspension clamp without dampers for Case-1, Case-2 and Case-3

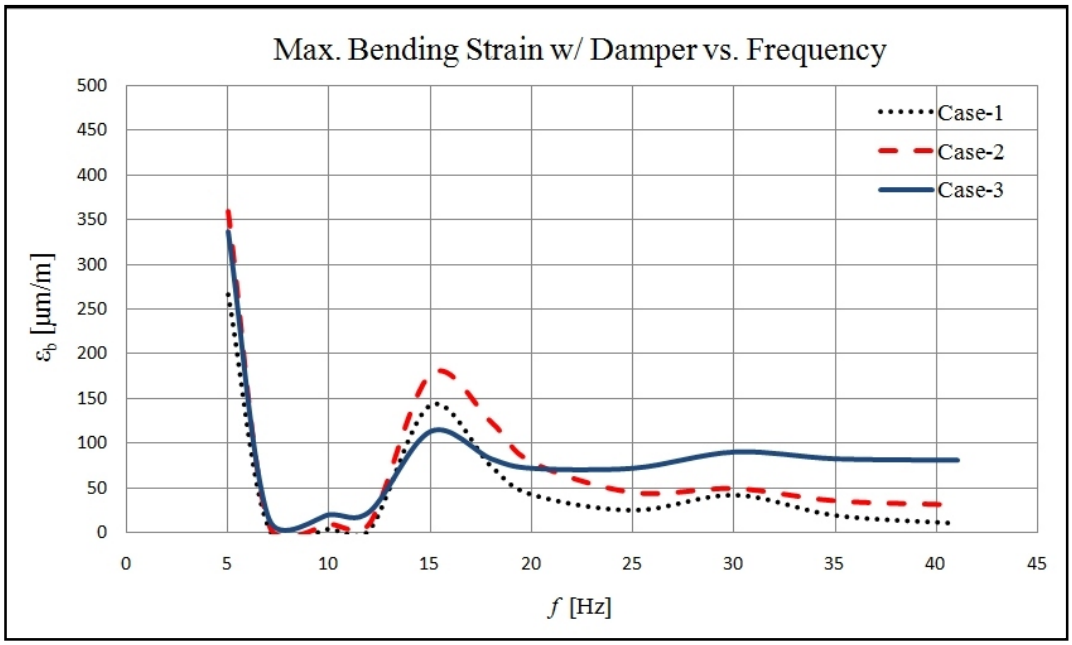

Figure 4.15 Computed max. strains of the conductor at the suspension clamp with dampers for Case-1, Case-2 and Case-3

As seen in Figure 4.14 and Figure 4.15, estimated maximum strains of the conductor at the suspension clamp have the same trend with the estimated maximum vibration amplitudes of the conductor due to their correlation formalized in the subsection 3.2.5. Optionally, previously computed values can be performed for a specific wind velocity by introducing the Stockbridge damper characterization test data at the lock-in frequency and sample calculations performed for the Case-2 are illustrated in Table 4.6. In addition, displacements along the conductor with and without damper plots can be reached in this computation option of the software as illustrated in Figure 4.16,

Table 4.6 Single lock-in frequency calculations

V_{wind} [m/s]	f [Hz]	A_{max} [mm] w/o dampers	A_{max} [mm] w/ dampers	B. Strain [μm/m] w/o dampers	B. Strain [μm/m] w/ dampers
1.5	9.1	21.22	0.36	484.9	8.3
3.0	18.3	4.43	2.62	202.4	119.5
4.5	27.4	1.19	0.59	81.8	41.0
6.0	36.5	0.47	0.37	43.2	33.6

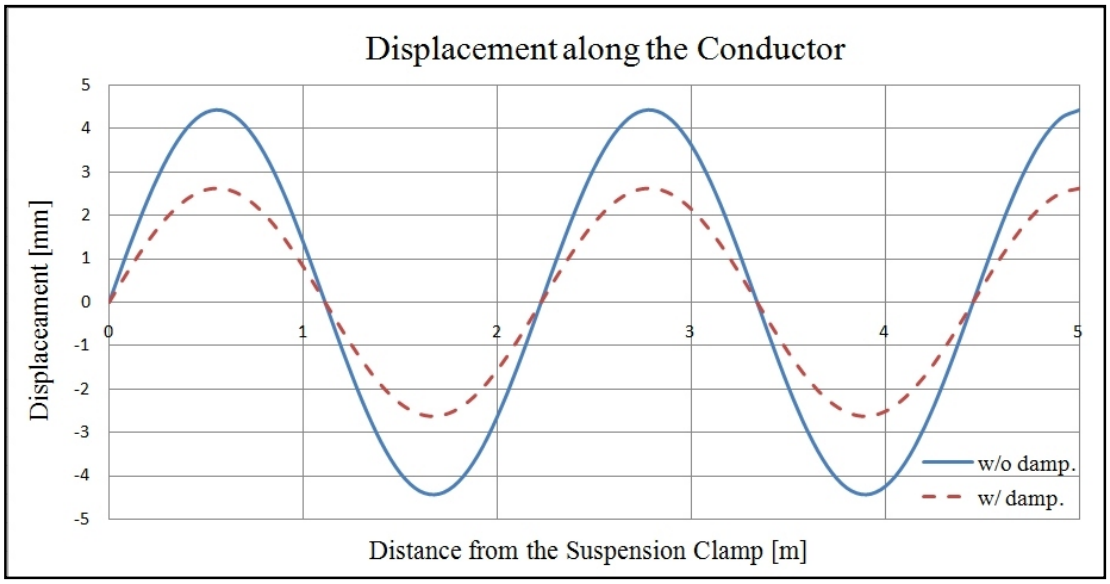

Figure 4.16 Displacements of the conductor for the first 5 *m* at 18.3 Hz which is in the wind velocity of 3 *m/s*

CHAPTER 5

DEVELOPMENT OF THE TEST SETUP

In this chapter, the conceptual and the detailed design of the test setup are discussed together with the modal and the transmissibility analyses. In the validation step of the test setup, performed transmissibility test is examined at the end of the chapter.

5.1 Conceptual Design

As mentioned previously, sample characterization tests, which the damping ability of the Stockbridge damper could be introduced to the software, are performed. For this purpose, due to its unavailability in the market, a test setup is designed by considering the target frequencies which are in the range of 3 to 150 *Hz* for the aeolian vibrations.

The aim of this test is measuring the velocity and the force data of the Stockbridge damper to reveal the power dissipation in the frequency domain. For this task, an accelerometer and a force transducer are used to measure the related test data and as required they are placed as possible as in the same line vertically with the clamp of the damper for the accuracy of the test. The details of this test are discussed in Chapter 6.

In the design steps, CAD models are prepared by using Pro/ENGINEER, modal and transmissibility analyses are performed through ANSYS Workbench. Regarding to

the conceptual design, the simplified models prepared by these packet programs are illustrated in Figure 5.1. The conceptual test setup consists of the setup base, the lower adaptor, the upper adaptor, the side walls, the accelerometer platform and the shaft parts. The setup base part is used to fasten the test setup to the shaker. Besides, the lower and the upper adaptors are designed to mount the force transducer between them. On the other hand, the accelerometer is placed on the accelerometer platform and the Stockbridge damper is placed on the shaft part. The simplified CAD model of the conceptual test setup is given in an exploded view in Figure 5.2.

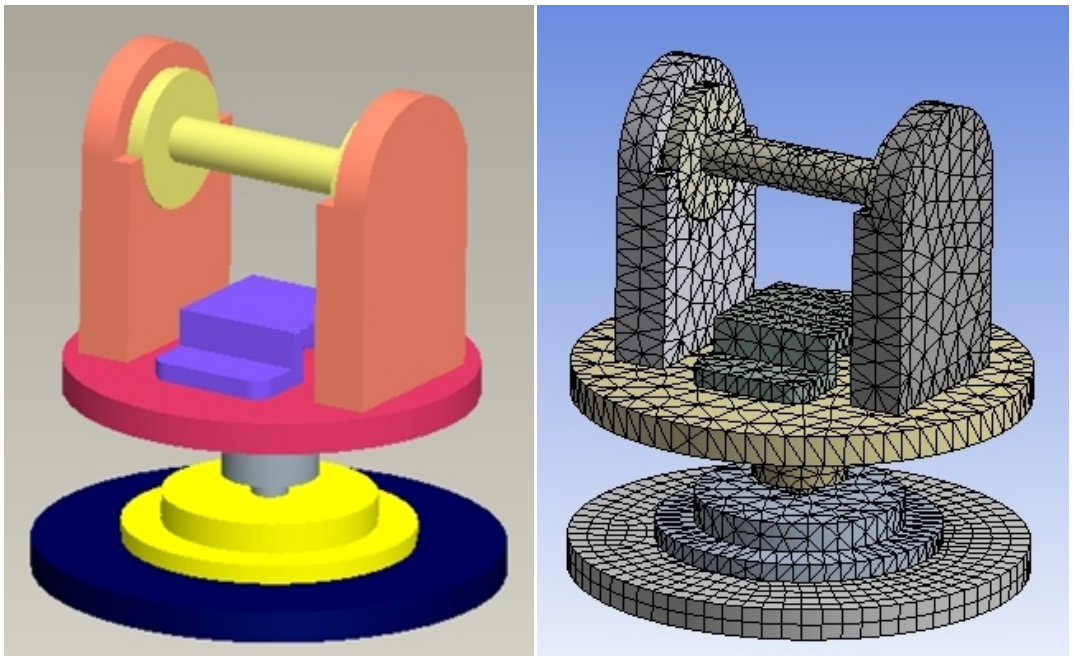

Figure 5.1 The simplified CAD model (left) and the meshed model (right) of the conceptual test setup for the modal analysis

In the modal analysis step, all of the parts are connected with bounded type of connections and the model is fixed from the bottom surface of the setup base part. The materials of the conceptual test setup parts are given in Table 5.1.

Table 5.1 The materials of the conceptual test setup parts

Part	Material
Setup Base	Aluminum 6061-T6
Lower Adaptor	303 Stainless Steel
Upper Adaptor	303 Stainless Steel
Accelerometer Platform	Aluminum 6061-T6
Side Walls	Aluminum 6061-T6
Shaft	303 Stainless Steel

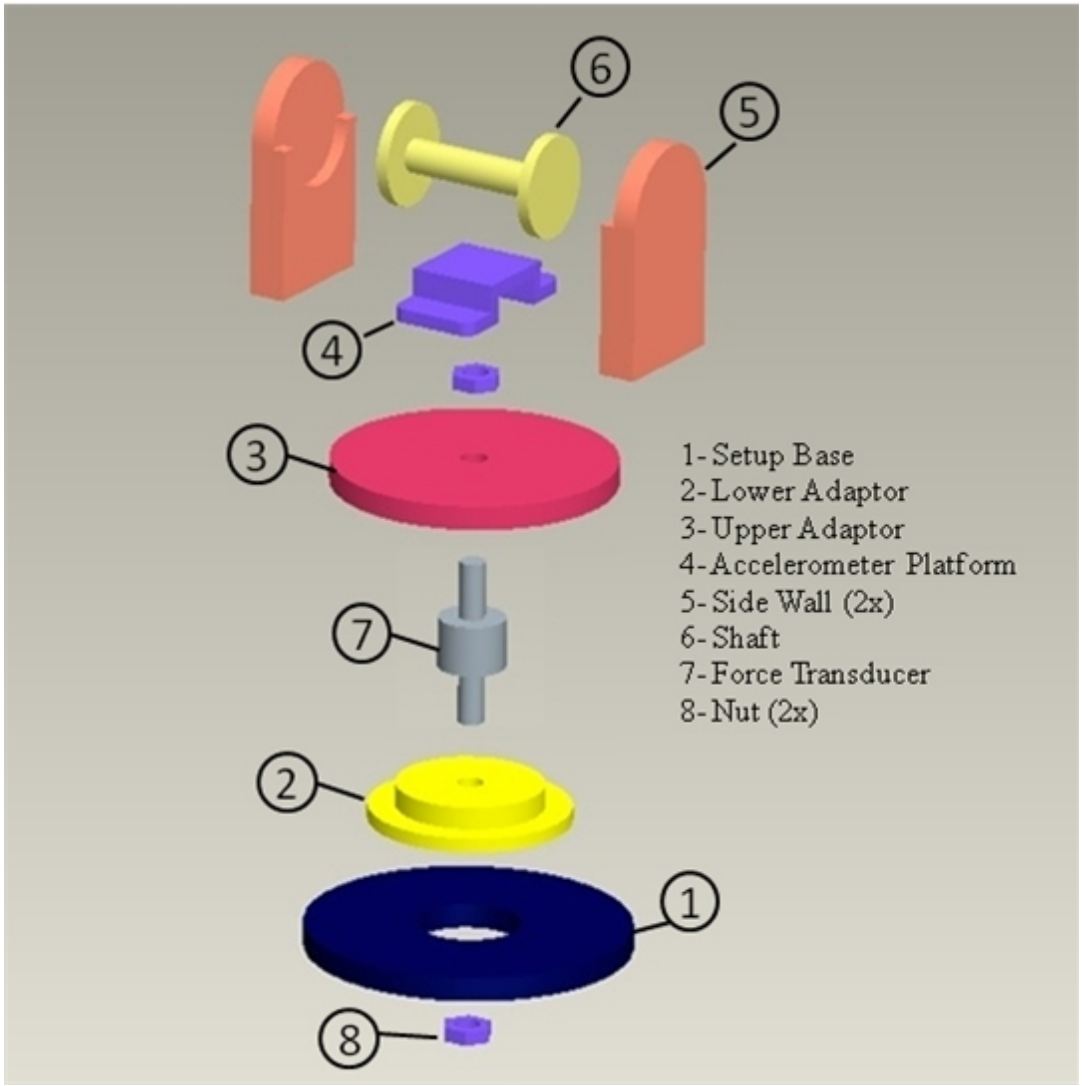

Figure 5.2 Exploded view for the simplified CAD model of the conceptual test setup

The modal analysis is performed with 10074 elements and 26680 nodes. SOLID186, which is a higher order 3-D solid element presenting quadratic displacement behavior, is used during the analysis. Examination of the modal analysis results reveals that the first and the second natural frequencies are 67.4 *Hz* and 71.4 *Hz* respectively. As seen in Figures 5.3 and 5.4, the first and the second mode shapes are similar and the need for supporting the upper adaptor is emerged to move up the first and the second natural frequencies above 150 *Hz*. The solution for this problem is discussed in the next subsection.

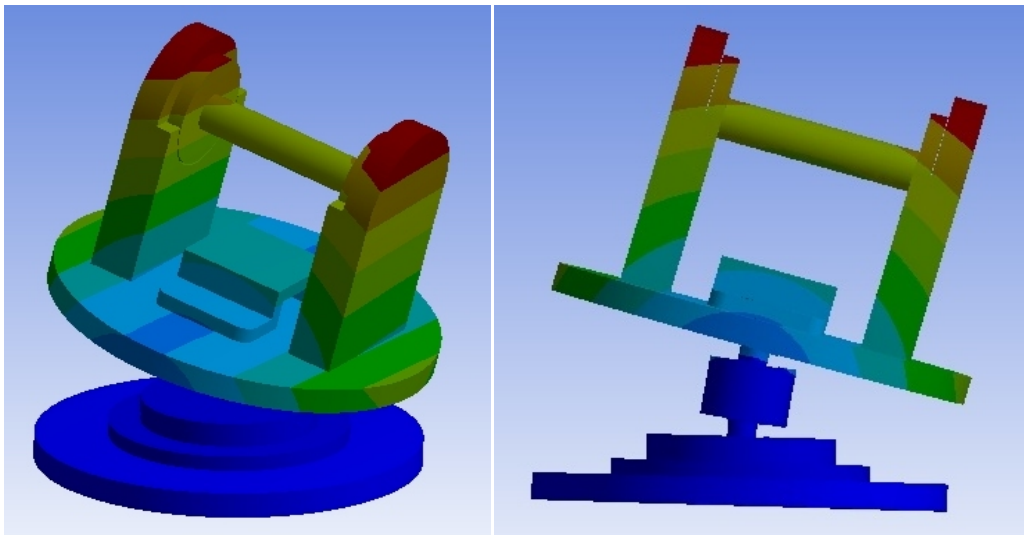

Figure 5.3 Isometric view (left) and front view (right) of the first mode shape of the conceptual test setup at 67.4 *Hz*

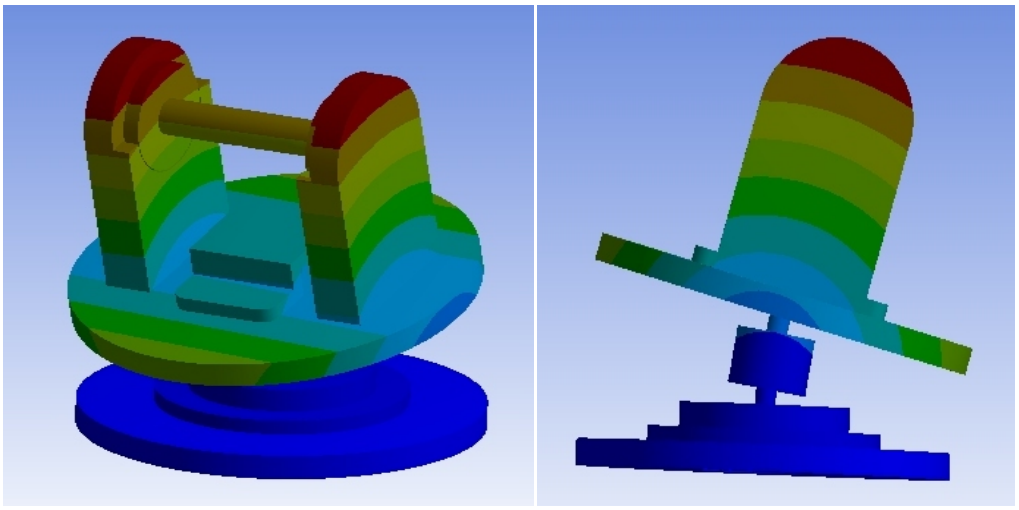

Figure 5.4 Isometric view (left) and side view (right) of the second mode shape of the conceptual test setup at 71.4 *Hz*

5.2 Detailed Design

To solve the emerged problem related with the first and the second natural frequencies in the conceptual design of the test setup, additional SKF LBCT type linear ball bearings are adopted to support the upper adaptor part as seen in Figure 5.6. For this purpose, the setup base and the upper adaptor parts are modified and the bearing rod parts, whose materials are also 303 type stainless steel, are designed additionally. The simplified CAD model of the modified test setup is given in an exploded view in Figure 5.5.

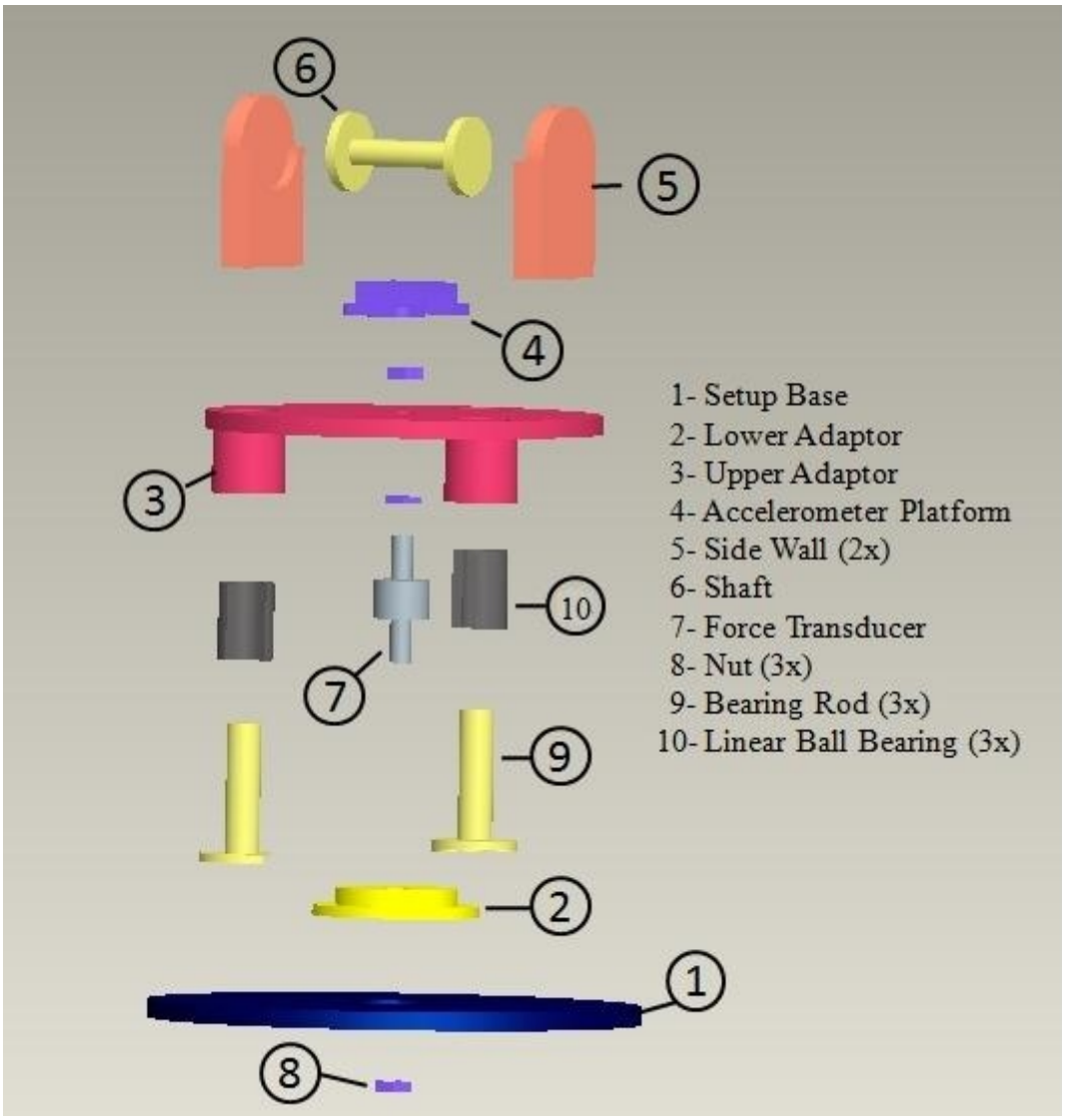

Figure 5.5 Exploded view for the simplified CAD model of the modified test setup

Figure 5.6 SKF LBCT type linear ball bearing

In the modal analysis step, all of the parts are connected with bounded type of connections except the connections between the linear ball bearings and the bearing rods. They are no separation type connections which allow the upper adaptor part to move vertically on the bearing rods. The model is fixed from the bottom surface of the setup base part as before and the modal analysis is performed with 12611 elements (SOLID186) and 38182 nodes. Regarding to the modified test setup, the simplified models prepared for the modal and transmissibility analyses are illustrated in Figure 5.7.

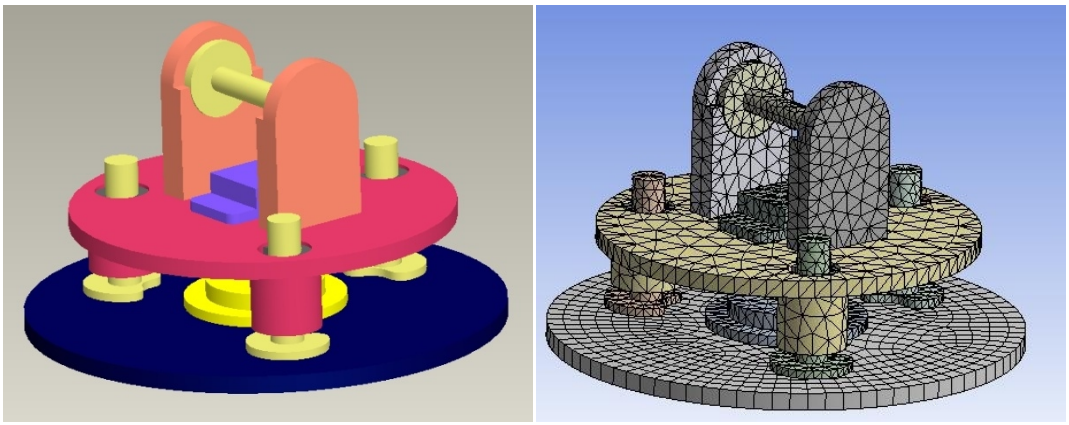

Figure 5.7 The simplified CAD model (left) and the meshed model (right) of the modified test setup for the modal and transmissibility analyses

When the results of the modal analysis are examined for the modified test setup, the first and the second natural frequencies are observed as 344.1 *Hz* and 352.0 *Hz* respectively at this time. As seen in Figures 5.8 and 5.9, the first and the second mode shapes are similar to those of the conceptual design but they occur at higher frequencies which are beyond the scope of this study.

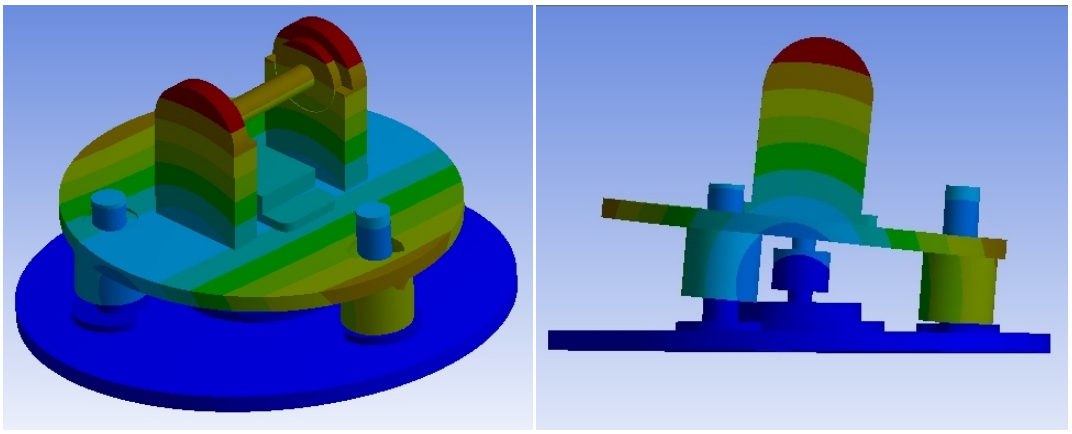

Figure 5.8 Isometric view (left) and side view (right) of the first mode shape of the modified test setup at 344.1 *Hz*

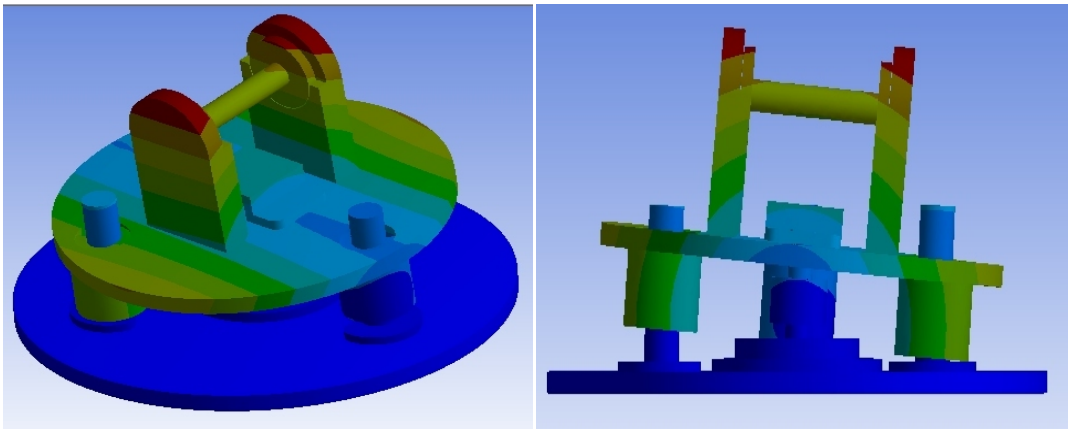

Figure 5.9 Isometric view (left) and front view (right) of the second mode shape of the modified test setup at 352.0 *Hz*

In addition, the random vibration tool of ANSYS Workbench is used to perform the transmissibility analyses of the points that are used to place the accelerometer and the clamp of the Stockbridge damper. The target points and the excitation surface for the transmissibility analyses are illustrated in Figure 5.10. The fixing surface, the meshing element type and the connection types of the parts are same with the modal

analysis of the modified test setup. The excitation is introduced in the type of PSD g acceleration which is 0.001 g^2 / Hz in the frequency range of 5 to 1000 *Hz*.

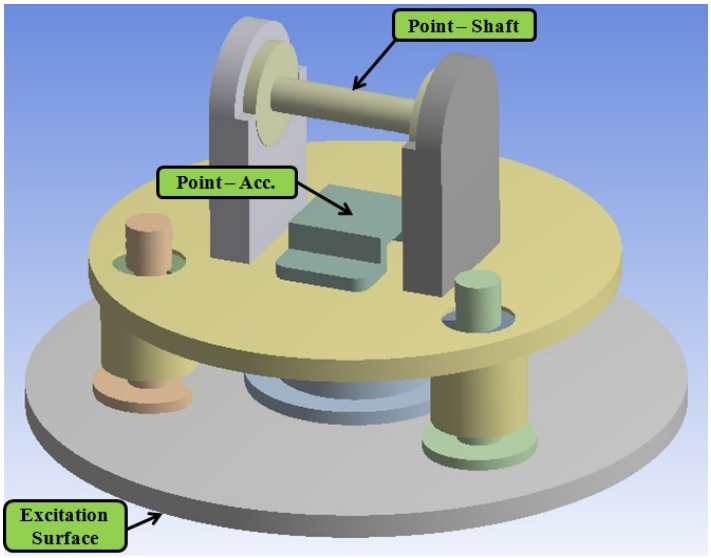

Figure 5.10 The excitation surface and the target points for the transmissibility analyses

When the results of the transmissibility analysis are examined, the transmissibility is about 1% up to 200 *Hz*. As seen in Figure 5.11, the results of the transmissibility analysis reveal that the target points appear to be convenient for the placement of the accelerometer and the Stockbridge damper during the characterization tests. In the light of undertaken analyses, it is proceeded with the validation of the test setup.

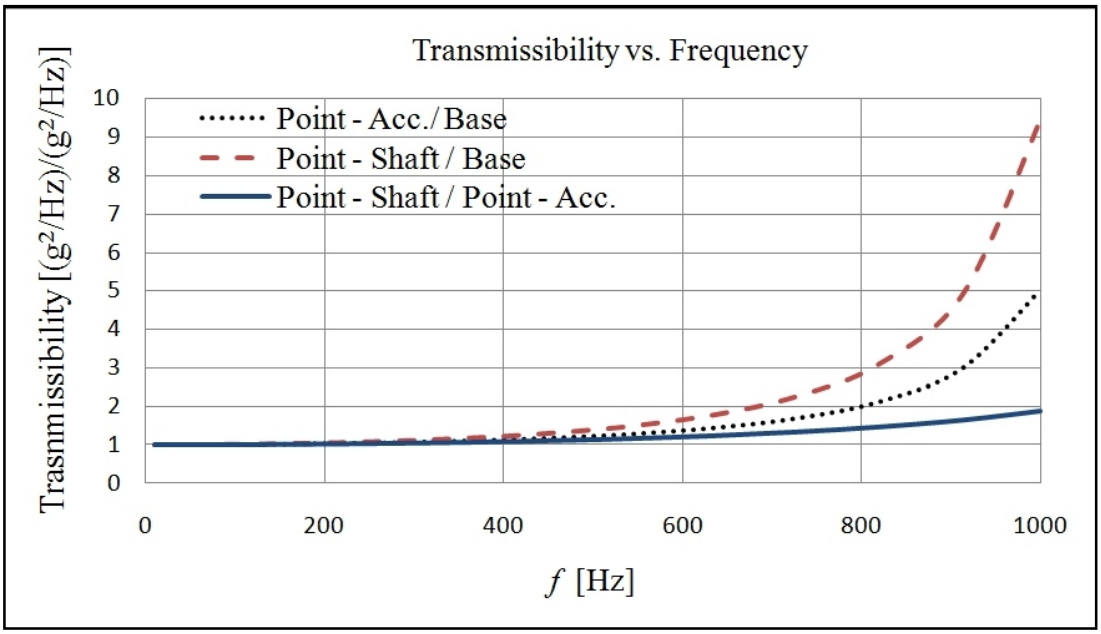

Figure 5.11 Results of the transmissibility analysis for the modified test setup

5.3 Validation of the Test Setup

Utilizing the results of the analyses the parts of the test setup are produced and assembled by using M5 screws as seen in Figure 5.12. M3 screws are also used only for the linear ball bearings to prevent their axial and tangential motion. The force transducer is placed between the upper and the lower adaptors by using its M10 nuts. The placement of the force transducer between the upper and lower adaptors can also be seen in Figure 5.12. The estimated total mass of the parts from the CAD models, which are placed on the force transducer, is 2.45 *kg* by Pro/ENGINEER. The mass of the produced and assembled set of parts on the transducer is 2.46 *kg* and the total mass of the test setup is 4.15 *kg*.

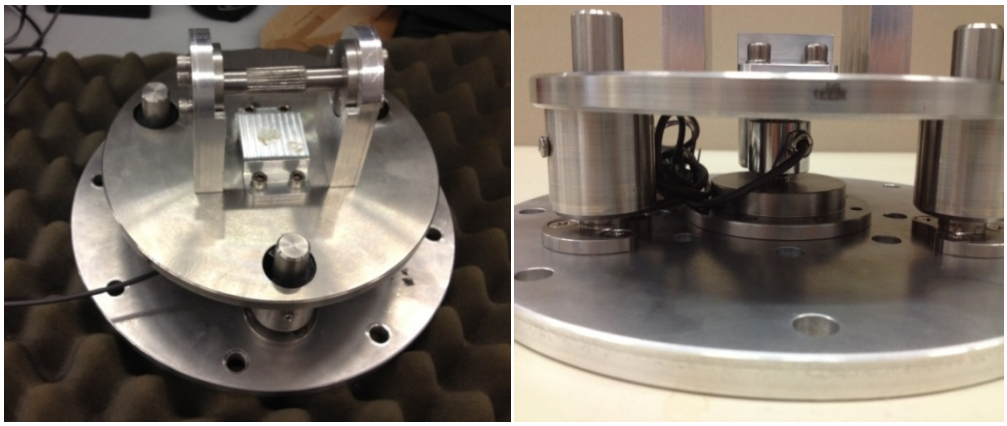

Figure 5.12 Assembled test setup (left) and the placement of the force transducer between the upper and the lower adaptors (right)

Transmissibility test is done on the same bases with the previously done transmissibility analysis and the accelerometers are placed as seen in Figure 5.13. The first accelerometer is placed on the setup base part while the second and the third one are placed on the accelerometer platform and the shaft parts respectively. There is another accelerometer in the test which is used by the shaker. The placements of the accelerometers are also tabulated in Table 5.2.

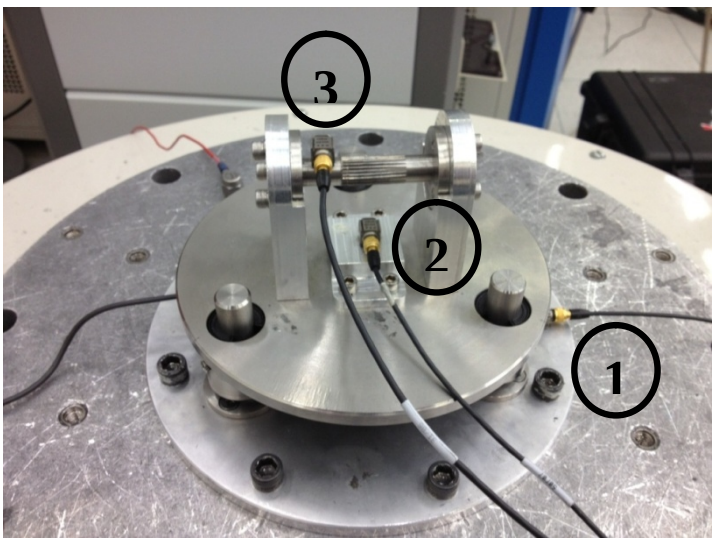

Figure 5.13 The placements of the accelerometers for the transmissibility test

Table 5.2 The placements of the accelerometers for the transmissibility test

Number	Serial No	Placement	Notation for the Plots
1	30253	Setup Base	Acc.1
2	31803	Accelerometer Platform	Acc.2
3	31802	Shaft	Acc.3

The excitation is introduced by the shaker in the type of PSD g acceleration which is 0.001 g^2 / Hz in the frequency range of 5 to 1000 *Hz*. It is observed that results of the transmissibility test are consistent with the transmissibility analysis where the transmissibility is about 1.2% in the range of 5 to 150 *Hz*. The transmissibility test results are in line with TR1, TR2 and TR3 up to 400 *Hz* however both TR1 and TR2 diverge from TR3 after 400 *Hz* substantially as seen in Figure 5.14.

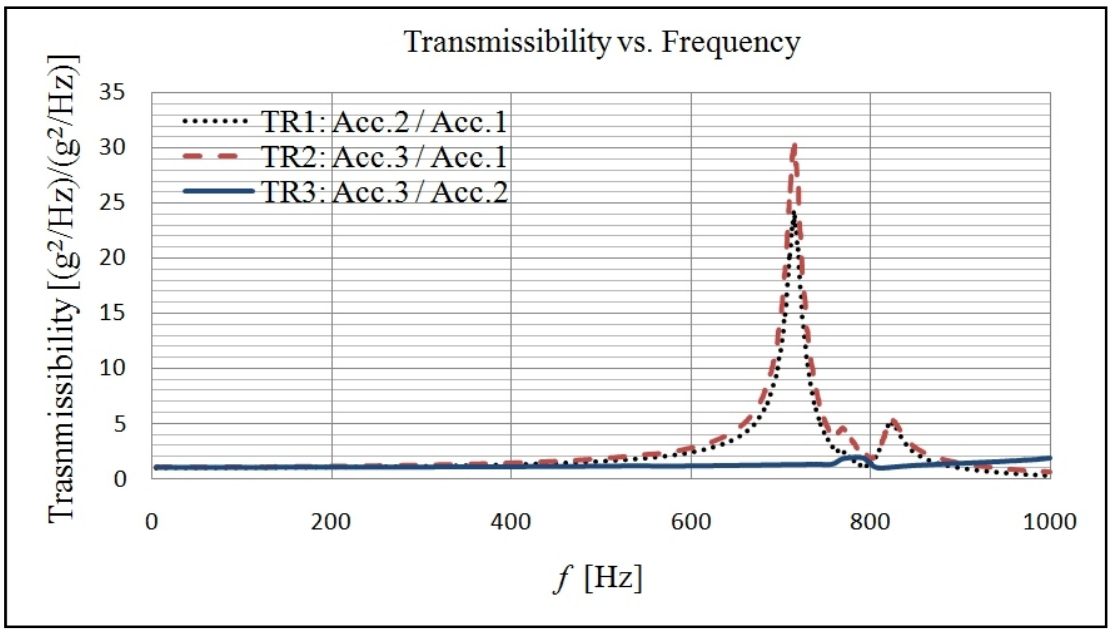

Figure 5.14 Results of the transmissibility test for the test setup

TR1 and TR2 make a noticeable peak at about 715 *Hz* and a modal test is performed for the upper adaptor to understand the reason behind this peak. For the modal test,

three accelerometers are placed on the upper adaptor part as seen in Figure 5.15 and the placements of the accelerometers are also tabulated in Table 5.3. The excitation introduced by the shaker is same with the transmissibility test.

Table 5.3 The placements of the accelerometers for the modal test

Number	Serial No	Placement
1	30253	Upper Adaptor - Front
2	31803	Upper Adaptor - Right
3	31802	Upper Adaptor - Left

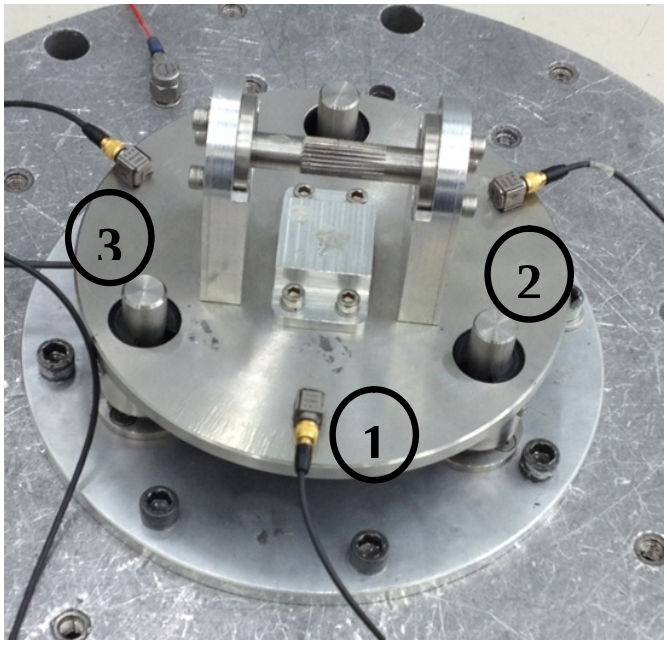

Figure 5.15 The placements of the accelerometers for the modal test

The positions of the accelerometers on the upper adaptor are simply introduced to Brüel & Kjaer Pulse Labshop and a simulation of the mode shape at the related frequency is generated by the software. The accelerometer placements introduced to

the software by its interface and a view from the mode shape simulation are given in Figure 5.16. The mode shape simulation represents that the upper adaptor moves in the vertical direction and this motion is crucial for the measurements of the force at that frequency.

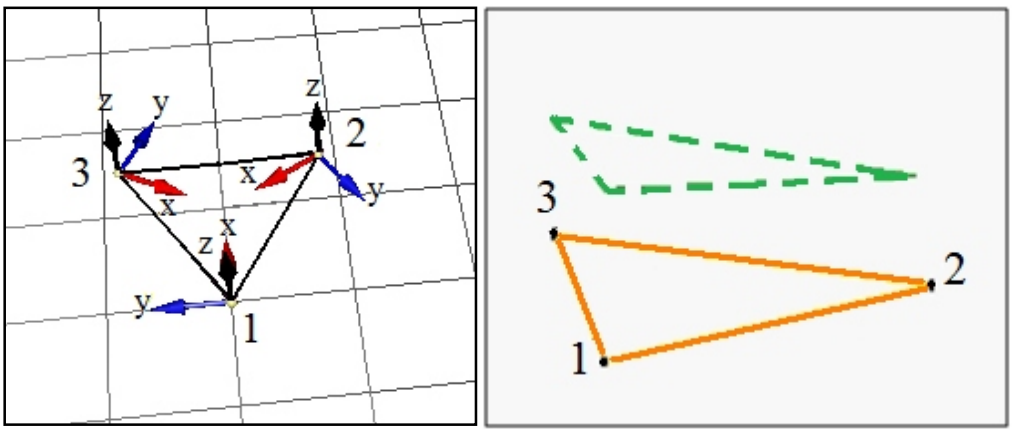

Figure 5.16 The introduced accelerometer placements (left) and a view from the mode shape simulation (right)

CHAPTER 6

THE STOCKBRIDGE CHARACTERIZATION TESTS

In this chapter, the procedure of the damper characteristic test, which is stated in the international standard IEC 61897, is explained. After a brief introduction of the test equipments, performed stepped-sine and swept-sine test are discussed for with and without damper cases and the comparison of the results are presented at the end of the chapter.

6.1 Damper Characteristic Test Procedure

According to the international standard IEC 61897 [5], unless a narrower frequency range is agreed between the purchaser and the supplier, a frequency range of $(0.18/D)$ to $(1.4/D)$ shall be covered. In the case of logarithmic sweep, any automatic sweep rate, which is not exceeding 0.2 *decade/min*, may be used. On the other hand, this rate is *0.5 Hz/s* in the case of linear sweep. Alternatively, the frequency range may be covered in the step intervals of 0.5 *Hz* up to 10 *Hz*, 1 *Hz* up to 100 *Hz* and 2 *Hz* above 100 *Hz*. In this case, the steady state condition of the test setup should be achieved at each frequency before the measurements.

The velocity of the Stockbridge damper clamp should be held constant at 0.1 *m/s* (single peak) during the Stockbridge damper characteristic test and the force applied by the damper is measured with a force transducer. The damper power [*W*] is determined as;

$$P_{char.} = 0.5 F_{damp.} V_{clamp} \cos\alpha \tag{6.1}$$

where $F_{damp.}$ is the force (peak value) [N], V_{clamp} is the velocity of the damper clamp [m/s] and α is the phase angle between the velocity and the force [°]. In this study, the stepped-sine and swept-sine tests are performed for the characteristic test of the Stockbridge damper.

6.2 Test Equipments

In the stepped-sine and swept-sine tests, LDS V875LS-440 air cooled vibrator is used as the excitation platform with its shaker control software. The test data is recorded by using DEWETRON-501 with the help of its software DEWESOFT. The test shaker and the data recorder are given in Figure 6.1.

Figure 6.1 LDS V875LS-440 air cooled vibrator (left) and DEWETRON-501 (right)

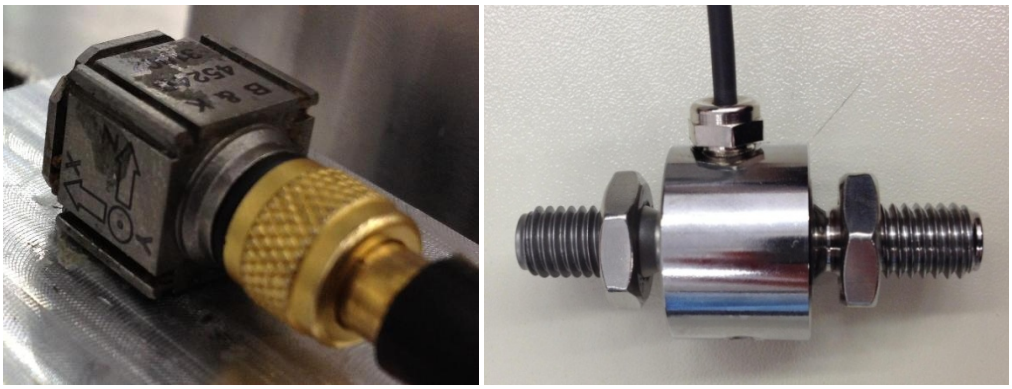

Figure 6.2 4524B accelerometer (left) and U9B force transducer (right)

Two kinds of sensors given in Figure 6.2, which are the accelerometers and the force transducer, are used in the damper characterization tests. The accelerometers are Brüel & Kjaer 4524B triaxial lightweight sensors and the force transducer is the HBM U9B which is capable of measuring tensile and compressive forces. The technical specifications of the sensors are given in Appendix A.

6.3 Stepped-Sine Tests

The stepped-sine test is performed two times with and without the Stockbridge damper. The accelerometer of the shaker is placed on the accelerometer platform to control the clamp velocity of the Stockbridge damper and the 4524B type accelerometer is also placed on the same platform to measure the related acceleration. The placements of the accelerometers for the damper characterization tests are given in Figure 6.3.

The stepped-sine test is performed between 5 *Hz* and 150 *Hz* in the frequency intervals of 1 *Hz*. After the test setup becomes steady state at 0.1 m/s (single peak), the force and the acceleration data is recorded for 4 seconds and then the shaker stops and waits for 10 seconds as seen in Figure 6.4.

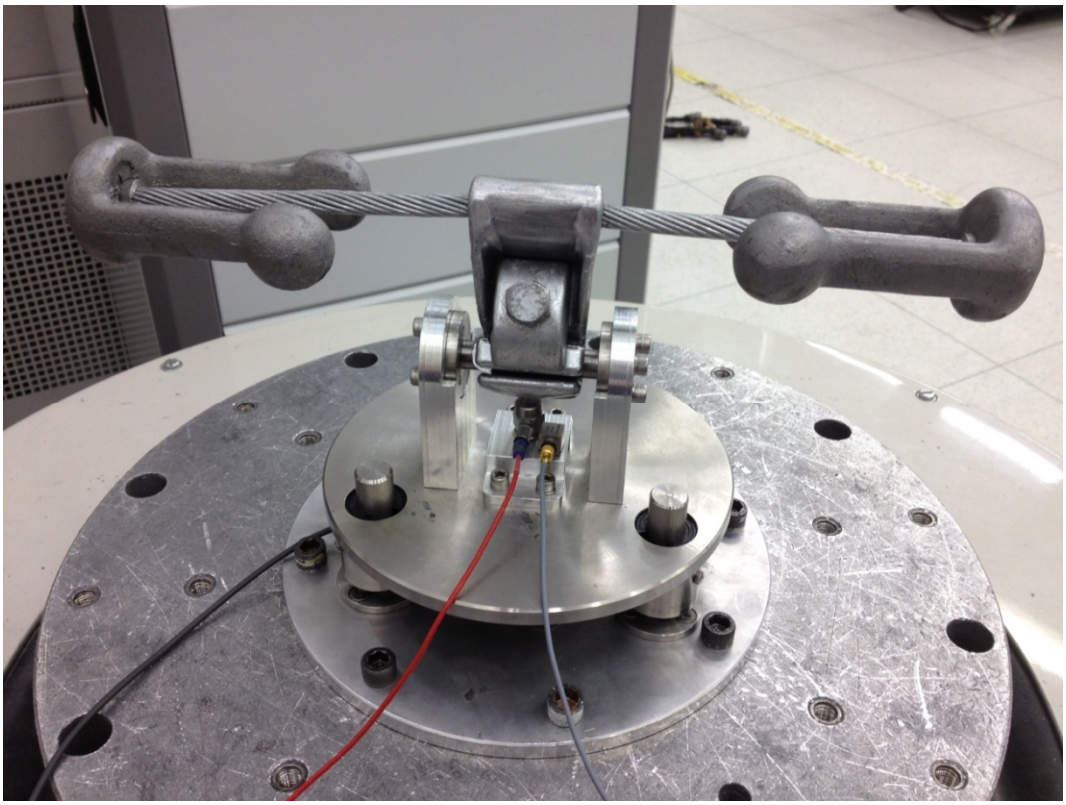

Figure 6.3 The placements of the accelerometers for the damper characterization tests

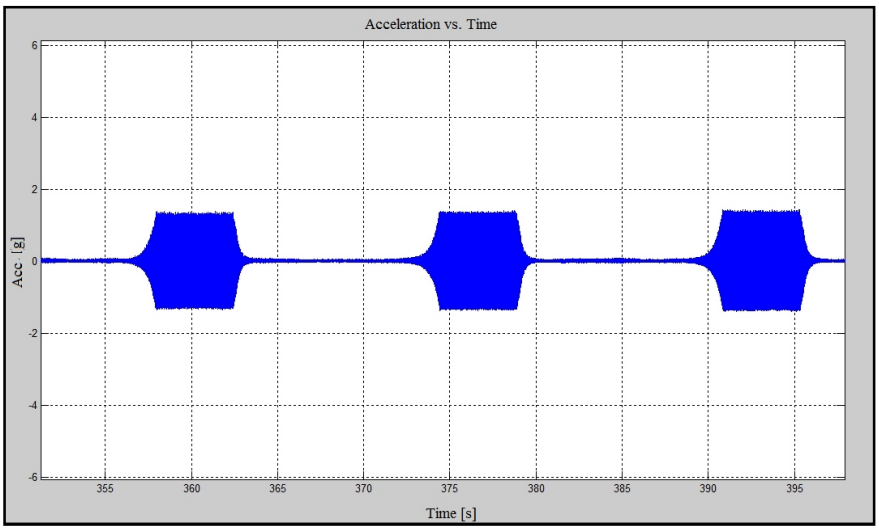

Figure 6.4 Acceleration *[g]* data recorded at 20 *Hz*, 21 *Hz* and 22 *Hz* during the stepped-sine test

For the post-processing of the test data, FFT function of MATLAB is used to convert the time domain test data to the frequency domain. This process is done for every four-seconds data and one of them is illustrated in Figure 6.5.

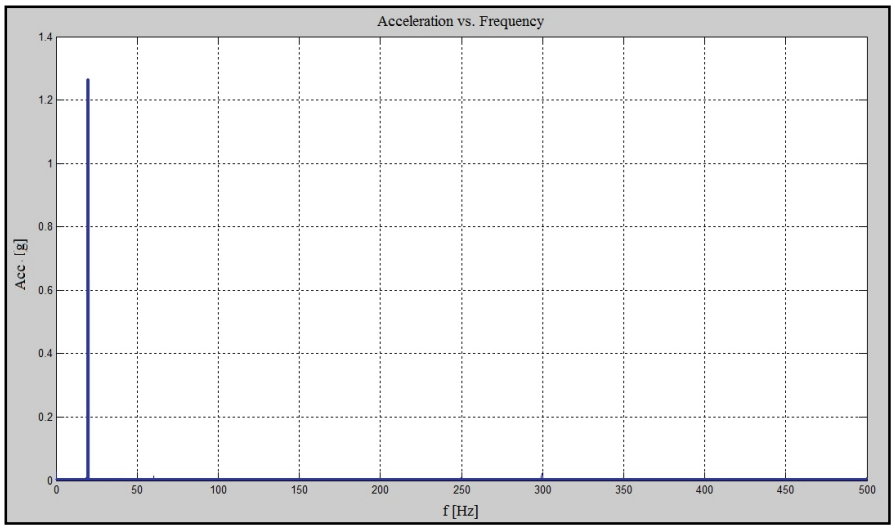

Figure 6.5 Acceleration *[g]* data at 20 Hz in the frequency domain

The velocities of the clamp are verified from the velocity data records of the shaker and also calculated from the acceleration data as seen in Figure 6.6. The same steps are ruling for the force data and the calculated damper power via equation (6.1) is given in Figure 6.7.

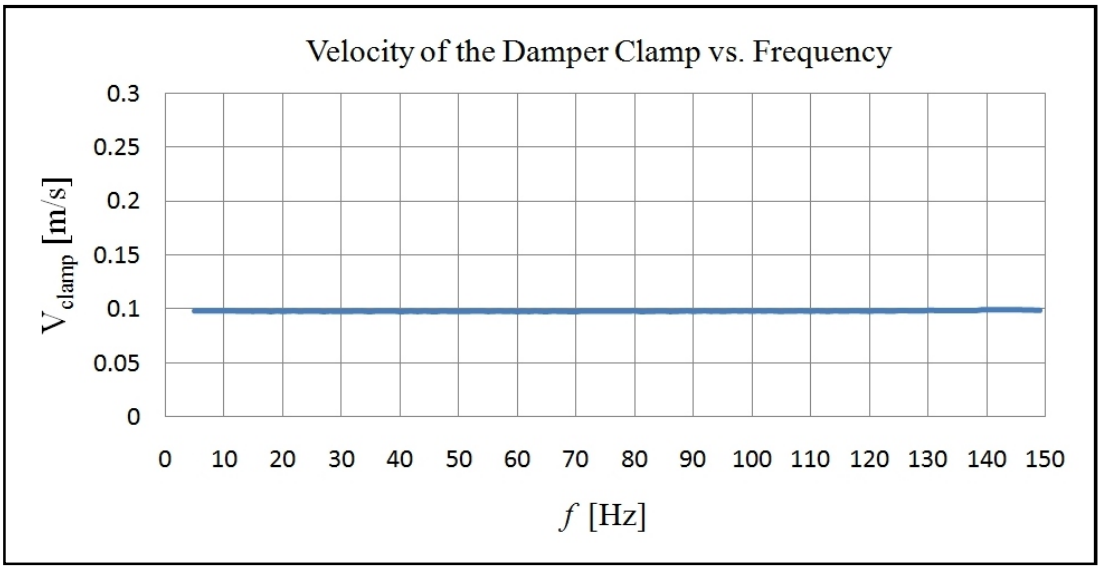

Figure 6.6 Velocity of the damper clamp in the frequency domain

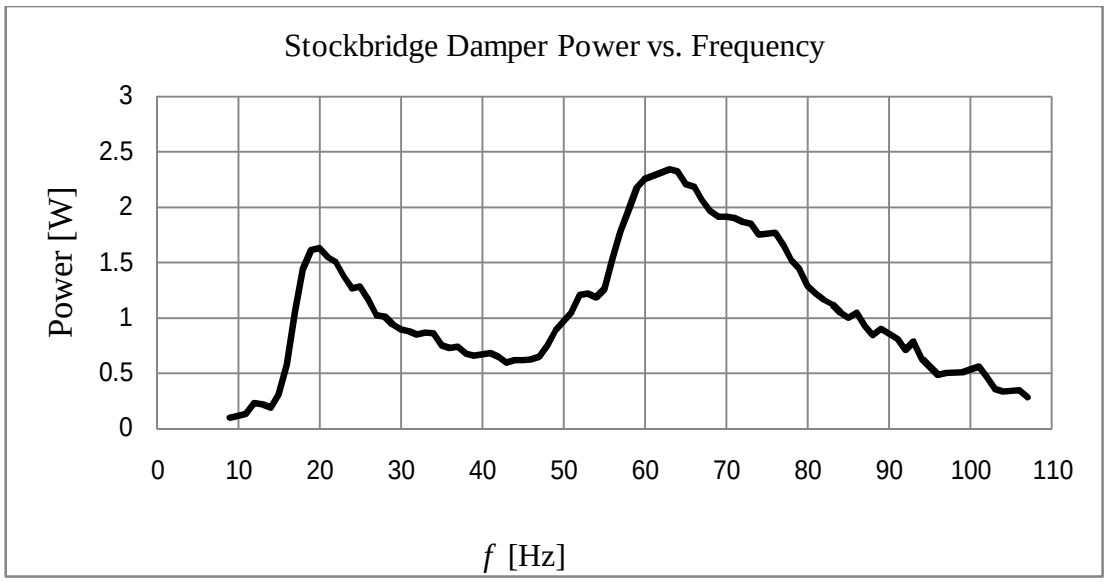

Figure 6.7 Power of the damper in the frequency domain

The second stepped-sine test is performed without the Stockbridge damper and the placements of the accelerometers are same with the first one as seen in Figure 6.8. The second stepped-sine is required for eliminating the negative effects of the linear

ball bearings and the power dissipation of the test setup. All of above steps are repeated for the test setup and the power curves can be seen in Figure 6.9.

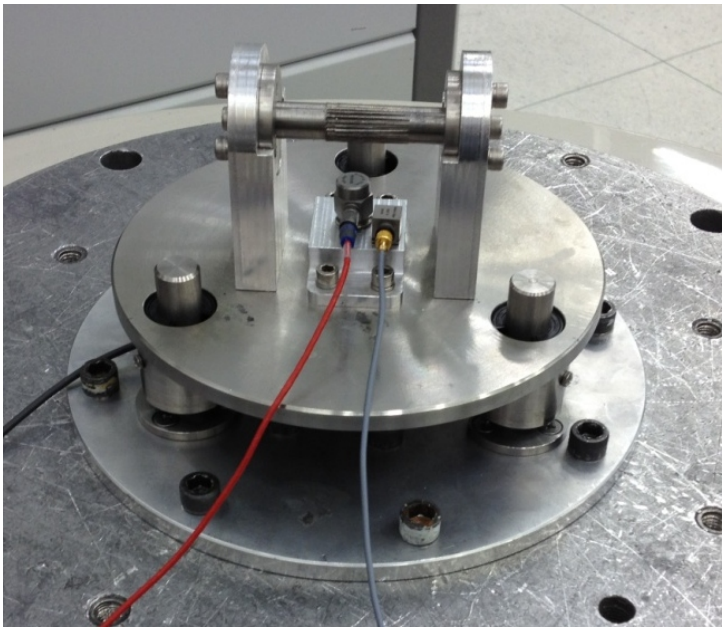

Figure 6.8 The characterization tests without the Stockbridge damper

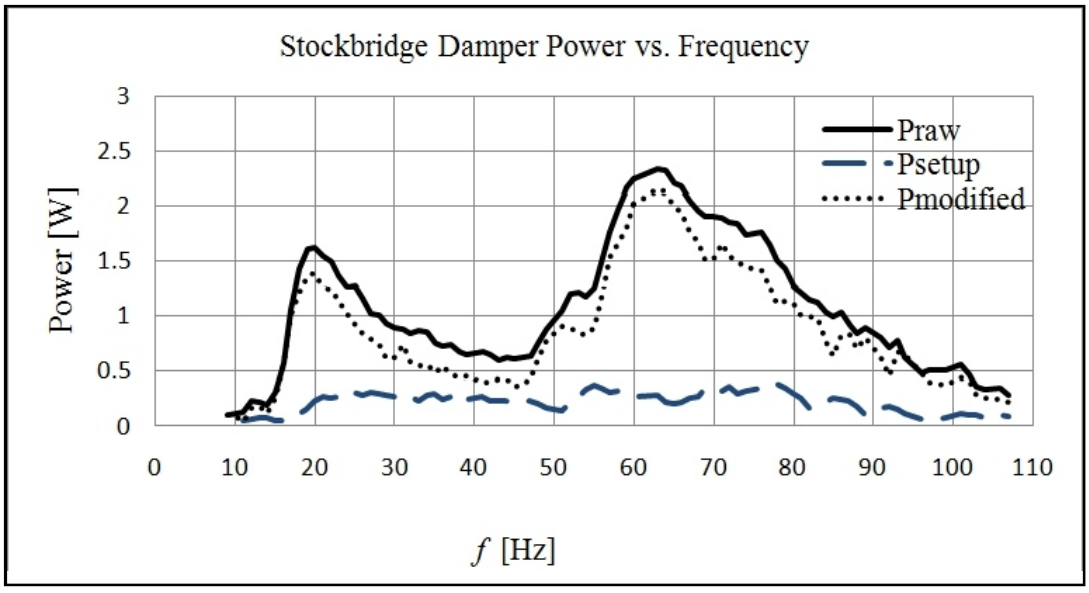

Figure 6.9 The raw damper power, modified damper power and power of the setup

6.4 Swept-Sine Tests

All of the discussions for the stepped-sine tests are valid for the swept-sine tests except the sweep rate. In this test, the logarithmic sweep rate of 0.2 *decade/min* is used to cover the frequency range. In addition, there is no duration time for the measurements as illustrated in Figure 6.10. A logarithmic sweep rate of 0.2 *decade/min* implies that the frequency is $10^{0.2}$ times the initial frequency after one minute and 10 times the initial frequency after 5 minutes.

The test results indicate that the damper power curves obtained by the stepped-sine and swept-sine tests are very close to each other as seen in Figure 6.11. When the damper power curves are examined, there are fluctuations both for the stepped-sine and the swept-sine tests because of the noise effects on the force transducer during the measurements. In addition, the characterization test to eliminate the negative effects of the linear ball bearings and the power dissipation of the test setup can be performed with an equivalent mass of the damper to observe the mass effect of the Stockbridge damper.

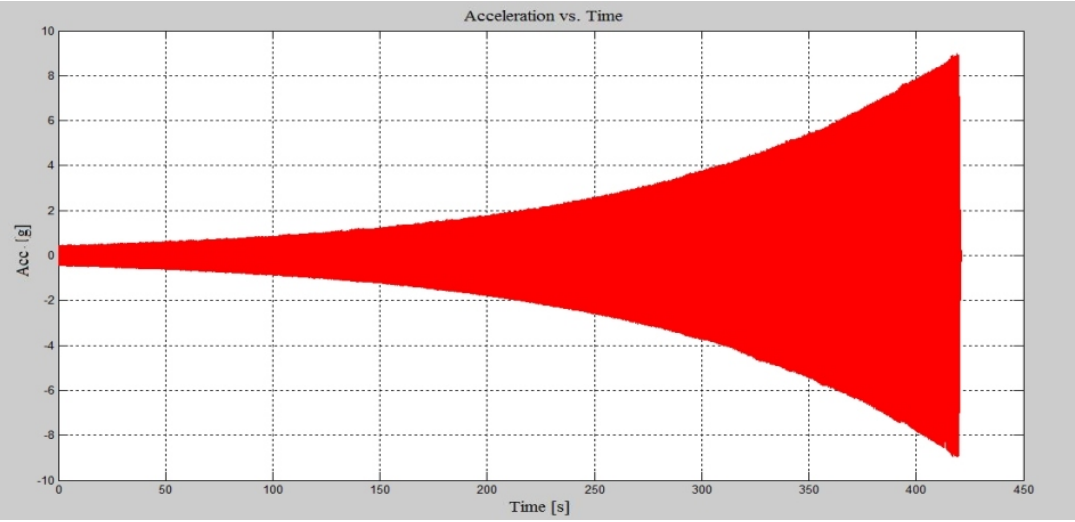

Figure 6.10 Acceleration *[g]* data recorded during the swept-sine test

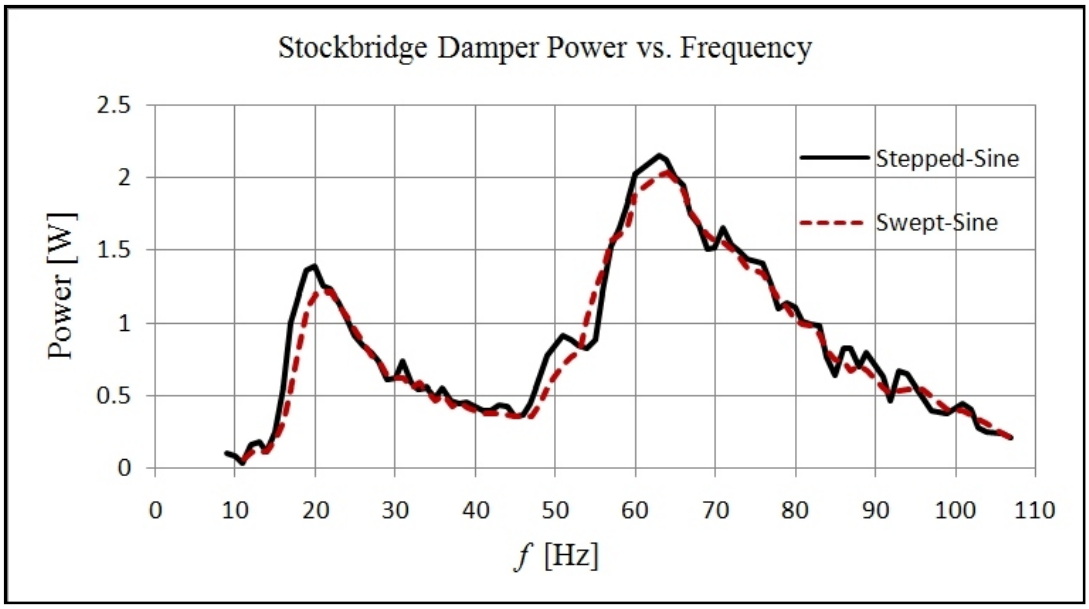

Figure 6.11 The damper power curves of stepped-sine and the swept-sine tests

CHAPTER 7

CONCLUSION

This thesis aims to examine the performance of Stockbridge dampers that are used to suppress aeolian vibrations on overhead transmission lines arising from the wind. In this respect, a program based on the Energy Balance Method is built up by MATLAB and validated further by existing field test results. Sample characterization tests, which require a test fixture design, are performed. In the design and validation steps of the test fixture, modal and transmissibility analyses are done by using ANSYS Workbench and the corresponding tests are performed in the laboratory.

As regards the developed software, a user friendly interface is built up by using GUI application of MATLAB. The interface allows the program to introduce the test characterization test results of the Stockbridge damper through two different options. The first option uses the characteristic test data file of the damper and the computations are performed in the range of wind velocities 1 to 7 *m/s*, while the second one provides computations for a specific wind velocity with the corresponding test values. The wind power is estimated by Riegert & Currie (1991) polynomial, Diana & Falco (1971) curve and the middle curve between Carroll (1936) and Diana & Falco (1971). On the other hand, Politecnico di Milano (2000), Tomkins (1956) and Claren & Diana (1969) are considered as the conductor self-damping exponents.

Once the software is developed, existing field tests are utilized for the validation of the software with and without damper cases. In addition to the field tests, the

performance of the above mentioned methods are evaluated further through various combinations to investigate the coherence between them. According to the results, all case studies appear to be in line with the validated combination, with the exception being the case based on Claren & Diana (1969) self-damping exponential constants. One of the cases is repeated by introducing specific wind velocities (the second option of the software) and the results indicate that both options can be used interchangeably.

Regarding the test setup required for the Stockbridge damper characteristic tests, due to its unavailability in the market, the test setup is designed by considering the target frequencies of the aeolian vibrations. In the design steps, CAD models are prepared through Pro/ENGINEER and modal and transmissibility analyses are performed via ANSYS Workbench. The results of the modal analysis of conceptual design justify that the first and the second natural frequencies are 67.4 *Hz* and 71.4 *Hz*, respectively. To solve the emerged problem related with the first and the second natural frequencies in the conceptual design of the test setup, additional linear ball bearings are adopted to improve the test setup. The modified test setup results uncover that the first and the second natural frequencies are 344.1 *Hz* and 352.0 *Hz*, respectively. In addition, the random vibration tool of ANSYS Workbench is used to perform the transmissibility analysis of the points used to place the accelerometer and the clamp of the Stockbridge damper. The results of the transmissibility analysis support convenience of the predetermined target points for the placement of the accelerometer and the Stockbridge damper for the characteristic test. All of these results ensure sufficiency to proceed with the production of the required parts of the test setup. Transmissibility test is done on the same bases with the transmissibility analysis and consistent results are obtained in the range of 5 to 150 *Hz* which are the target frequencies of the aeolian vibrations.

Finally, the stepped-sine and swept-sine tests are performed with and without damper for the characterization test of the Stockbridge damper. Tests without damper are

used to eliminate the negative effects arising from the linear ball bearings and the power dissipation of the test setup. As expected, the test results indicate that the damper power dissipation curves are very close to each other for the both tests.

For further research, the finite element model of the Stockbridge damper and the conductor with the aerodynamic flow effects of the wind could be generated to simulate the field tests used in the validation step. As another direction for further research, the bundled conductors could be taken into account for the performance evaluation of the Stockbridge dampers. Furthermore, the software could be improved to calculate the optimal position of the Stockbridge damper on the conductors in order to gain the maximum efficiency for a specific environmental condition.

REFERENCES

[1] Wikipedia, “Stockbridge Damper”, http://en.wikipedia.org/wiki/Stockbridge_ damper, Last visited 10 May 2012.

[2] Preformed Line Products, “Transmisson Repair Manual”, March 2010.

[3] Morgan V. T., ”The Detection and Damping of Overhead-Line Conductor Vibration”, The Institution of Electrical Engineers, no. 3885 M, June 1962.

[4] Dulhunty P. W., “Vibration Dampers – An Evolution in Australia”, http://www.dulhunty.com/an1.htm, Last visited 10 August 2012.

[5] IEC 61897 Ed. 1.0, “Requirements and Tests for Stockbridge Type Aeolian Vibration Dampers”, 1998.

[6] IEEE Std 1368-2006, “IEEE Guide for Aeolian Vibration Field Measurements of Overhead Conductors”, 2006.

[7] EPRI, “Updating the EPRI Transmission Line Reference Book: Wind-Induced Conductor Motion (The Orange Book)”, 2005 Progress Report, 1010223, CA, (2005).

[8] IEEE Std 664-1980, “IEEE Guide on the Measurement of the Performance of Aeolian Vibration Dampers for Single Conductors”, 1980.

[9] IEEE Std 563-1978, “IEEE Guide on Conductor Self-Damping Measurements”, 2007.

[10] Cernin K., “Reconstruction of Conductor Movement and Monitoring of High Voltage Lines”, BRNO University of Technology, Master’s Thesis, Brno 2009.

[11] Wang J. J., "Overhead Conductor Vibrations and Control Technologies", 2006 International Conference on Power System Technology, 2006.

[12] Vecchiarelli J., "Aeolian Vibration of a Conductor with a Stockbridge-Type Damper", Doctor of Philosophy Dissertation in Mechanical and Industrial Engineering, University of Toronto, Canada, 1997.

[13] Supreme & Co., "Design and Testing of Stockbridge Vibration Dampers", http://www.supreme.in/literatures.aspf, Last visited 12 June 2012.

[14] Sunkle D. C., Olenik J. J. and Fullerman M. D., "Determination of Damping Effectiveness of Impact Damper on ADSS Cable", Preformed Line Products, Ohio, 2000.

[15] Preformed Line Products, "Aeolian Vibration Basics", November 2008.

[16] Belloli M., Collina A. and Resta F., "Cables Vibrations due to Wind Action", Politecnico di Milano, O.I.T.A.F. Seminar, Grenoble, April 2006.

[17] Hill S., Snyder S. and Cazzolato B., "An Adaptive Vibration Absorber", Annual Conference of the Australian Acoustical Society, Adelaide, Australia, November 2002.

[18] Koo J.-H., Shukla A. and Ahmadian M.,"Dynamic Performance Analysis of Non-linear Tuned Vibration Absorbers", Communications in Nonlinear Science and Numerical Simulation, 13, 1929–1937, 2007.

[19] Nashif A.D., Jones D.I.G. and Henderson J.P., "Vibration Damping", Wiley Interscience, New York, 1985.

[20] Saidi I., Gad E. F., Wilson J. L. And Haritos N., "Development of Passive Viscoelastic Damper to Attenuate Excessive Floor Vibrations", Engineering Structures, 33, 3317-3328, 2011.

[21] Tigli O. F., "Optimum Vibration Absorber (Tuned Mass Damper) Design for Linear Damped Systems Subjected to Random Loads", Journal of Sound and Vibration, 331, 3035–3049, 2012.

[22] Stockbridge G. H., "Vibration Damper", US patent 16753913, July 1928.

[23] Li L., Kong D.-Y., Long X.- H. and Fanq Q.-H, "Numerical Analysis on Aeolian Vibration of Transmission Lines with Stockbridge Dampers", Journal of Chongqing University, December 2008.

[24] Sauter D., "Modeling the Dynamic Characteristics of Slack Wire Cables in Stockbridge Dampers" Doctor of Philosophy Dissertation in Mechanical Engineering, Technische Uni. Darmstadt, Darmstadt, 2003.

[25] Cloutier L. and Leblond A., "Fatigue Endurance Capability of Conductor/Clamp Systems Update of Present Knowledge", Technical Brochure Presentation to SC B2, Helsinki, July 2007.

[26] Havard D. G., "Fatigue of Conductors", Conductors and Accessories WG Meeting Presentation, FL, January 2010.

[27] Braga G. E., Nakamura R. And Furtado T. A., "Aeolian Vibration of Overhead Transmission Line Cables: Endurance Limits" 2004 IEEWPES Transmission 8 Distribution Conference & Exposition, 2004.

[28] The Engineering Tool Box, "Strouhal Number", http://www.engineering toolbox.com/strouhal-number-d_582.html, Last visited 15 July 2012.

[29] Kraus M. and Hagedorn, "Aeolian Vibrations: Wind Energy Input Evaluated from Measurements on an Energized Transmission Line", IEE Transactions on Power Delivery, vol.6, no. 3, July 1991.

[30] Verma H., "Aerodynamic and Structural Modeling for Vortex-Excited Vibrations in Bundled Conductors", Doctor of Philosophy Dissertation in Mechanical Engineering, Technische Uni. Darmstadt, Darmstadt, 2008.

[31] CIGRE SC22 EG22-11, "Modelling of Aeolian Vibration of Single Conductor: Assessment of the Technology", ELECTRA, vol. 181, 53-69, December 1998.

[32] Migdalovici M, Onisoru J., Videa E. and Albrecht A., "Finite Element Method for Control of Vibration of Overhead Line Conductors", SISOM, Bucharest, May 2004.

[33] Wolf H., Adum B., Semenki D. And Pustaic D., "Using the Energy Balance Method in Estimation of Overhead Transmission Line Aeolian Vibrations", Strojarstvo, 50 (5), 269-276, 2008.

[34] Guerard S., Godard B. and Lilien J.-J., "Aeolian Vibrations on Power-Line Conductors, Evaluation of Actual Self Damping", IEE Transactions on Power Delivery, vol. 26, no. 4, October 2011.

[35] IEC 62567 Ed. 1.0, "Methods for Testing Self-Damping Characteristics of Stranded Conductors for Overhead Lines", 2010.

[36] Liu X., "Cable Vibration Considering Internal Friction", Master of Science in Mechanical Engineering, University of Hawai'i, Manoa, USA, August 2004.

[37] Leblond A. and Hardy C., "Assessment of Safe Design Tension with Regard to Aeolian Vibrations of Single Overhead Conductors", The Institute of Electrical and Electronics Engineers, 2000.

[38] Diana G., "Modeling of Aeolian vibrations of single conductors and single conductors plus dampers", CIGRE presentation, Bangkok, February 2011.

[39] Eland Cables, "ACSR Conductor", http://www.eland.co.uk/documents/ACSR %20 - %20 Aluminium %20 Conductor %20Steel %20 Reinforced.pdf, Last visited 12 July 2012.

[40] Taihan Electric Wire Co. Ltd., "AL Conductors Catalog", http://www.taihan.com/en/product/downloader.asp?prodCatalogId=44&prodCatalogFileTy=F, Last visited 20 July 2012.

[41] HBM Test and Measurements, "U9B - Miniature Load Cell", http://www.hbm.com/en/menu/products/transducers-sensors/force/u9b, Last visited 12 May 2012.

[42] Brüel & Kjaer, "4524B – Cubic Triaxial DeltaTron Accelerometer", http://www.bksv.com/Products/transducers/vibration/accelerometers/accelerometers/ 4524B001.aspx?tab=specifications, Last visited 18 May 2012.

APPENDIX A

SPECIFICATIONS OF THE SENSORS

Table A.1 Technical specifications of U9B force transducer [41]

Type			U9B									
Nominal (rated) force	F_{nom}	N	50	100	200							
		kN				0.5	1	2	5	10	20	50
Nominal (rated) sensitivity	C_{nom}	mV/V	1									
Accuracy class			0.5									
Relative sensitivity error	d_C	%	≤ ±1 tension / ≤ ±2 compression									
Relative reproducibility error with unchanging mounting position	b_{rg}	%	≤ ±0.5									
Zero signal error	$(d_{s,0})$	mV/V	±0.075			±0.2						
Relative reversibility error (at 0.5 F_{nom})	$v_{0.5}$	%	≤ ±0.5									
Relative linearity error	d_{lin}	%	≤ ±0.5									
Relative creep over 30 min	d_{crF+E}	%	≤ ±0.2									
Effect of temperature on the sensitivity per 10 K in the nominal (rated) temperature range in the operating temperature range	TK_C	%	≤ ±0.5 ≤ ±0.8									
Effect of temperature on the zero signal per 10 K in the nominal (rated) temperature range in the operating temperature range	TK_0	%	≤ ±0.5 ≤ ±0.8									
Output resistance	R_a	Ω	300 … 400			<350						
Input resistance	R_e	Ω	>345			300 … 400						
Insulation resistance	R_{is}	GΩ	$>10^9$									
Reference excitation voltage	U_{ref}	V	5									
Operating range of excitation voltage	$B_{U,G}$	V	0.5 … 12									
Reference temperature	T_{ref}	°C [°F]	+23 [+73.4]									
Nominal (rated) temperature range	$B_{T,nom}$	°C [°F]	−10 … +70 [+14 … +158]									
Operating temperature range	$B_{T,G}$	°C [°F]	−30 … +85 [−22 … +185]									
Storage temperature range	$B_{T,S}$	°C [°F]	−30 … +85 [−58 … +185]									
Maximum operating force	(F_G)	% of F_{nom}	120									
Breaking force	(F_B)		>200									
Static lateral force limit [1]	(F_Q)		40					20				
Nominal (rated) displacement ±15 %	s_{nom}	mm	<0.1			0.04		0.06	0.09	0.11	0.13	
Fundamental resonance frequency ±15 %	f_G	kHz	7.3	10	15.7	15.5	23.7	18.7	20	23	27.8	20
Permissible oscillatory stress (vibration bandwidth per DIN 50100)	F_{rb}	% of F_{nom}	70									40
Weight, approx.		g	75			100						400
Degree of protection per DIN EN 60529			IP67									
Cable length		m	1.5									

Table A.2 Technical specifications of 4524B accelerometer [42]

	Units	4524	4524 B
Dynamic Characteristics			
Voltage Sensitivity (@ 159.2 Hz)	mV/ms^{-2} (mV/g)	10 ± 5% (100^{+3}_{-7}%)	
Measuring Range	ms^{-2} (g)	±500 (±50)	
Frequency Response		See typical Amplitude Response (Fig. 8)	
Mounted Resonance Frequency	kHz	x: 18 y: 9 z: 9	
Amplitude Response ±10%	Hz	x: 0.2 to 5500 y: 0.25 to 3000 z: 0.25 to 3000	
Phase Response ±5°	Hz	1.5 to 3000	
Temperature Response	%/°C (%/°F)	0.14 (0.08)	
Residual Noise (1 to 6000 Hz)	mg	x: < 0.4 y: < 0.2 z: < 0.2	
Transverse Sensitivity	%	< 5	
Electrical Characteristics			
DC Output Bias Voltage	V DC	+12 ±1	+13 ±1
Output Impedance	Ω	<2	<30
Grounding		Insulated from case	
Power Requirements		**Note: All three axes must be powered during operation**	
Supply Voltage	V DC	24 to 30	
Supply Current	mA	2 to 10	
Warm-up Time (90% of stabilised bias)	s	10	
Environmental Characteristics			
Temperature Range	°C (°F)	–54 to +100 (–65 to +212)	
Humidity		Hermetic	
Max. Operational Sinusoidal Vibration (peak)	ms^{-2} (g)	5000 (500)	
Max. Operational Shock (± peak)	ms^{-2} (g)	50000 (5000)	
Base Strain Sensitivity	Equiv. ms^{-2}/μ strain (g/μ strain)	Mounted in clip: 0.0005 (0.00005) Cemented to measuring object: 0.02 (0.002)	
Thermal Transient Sensitivity	Equiv. ms^{-2}/°C (g/°F)	0.004 (0.002)	
Magnetic Sensitivity (50 Hz–0.03 Tesla)	ms^{-2}/T (g/T)	20 (2)	
Physical Characteristics			
Dimensions		See outline drawing (Fig. 9)	
Weight	gram (oz.)	4.4 (0.15)	4.8 (0.17)
Case Material		Titanium	
Connector		Hermetic 4-pin receptacle ¼–28 UNF-2A	
Mounting		Adhesive or clip	